Cell Reports

Article

Single-cell transcriptomics of NRAS-mutated melanoma transitioning to drug resistance reveals P2RX7 as an indicator of early drug response

Graphical abstract

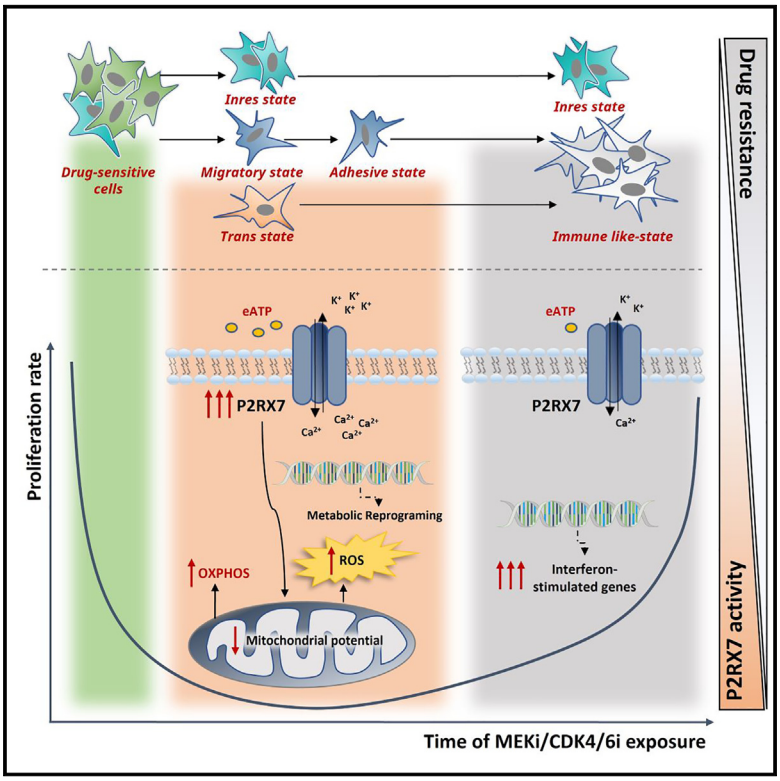

Highlights

- Ion signaling signature is enriched in early treated and static *NRAS*-mutant melanoma cells
- The activation of P2RX7 enhances the efficacy of combined MEK and CDK4/6 inhibitors
- Once resistant, cells re-enter the cell cycle and express immune-response-related genes
- An intrinsically resistant population is identified in both fast and slow adaptive cells

Authors

Tijana Randic, Stefano Magni, Demetra Philippidou, ..., Katrin B.M. Frauenknecht, Alexander Skupin, Stephanie Kreis

Correspondence

stephanie.kreis@uni.lu

In brief

Randic et al. elucidate the heterogeneity of *NRAS*-mutant melanoma cells following drug exposure and the transition to a drug-resistant state. Molecular programs related to transmembrane transport and migration, among others, define the slow proliferating melanoma state. The transcriptional landscape shifts toward an immune response signature during prolonged treatment.

Randic et al., 2023, Cell Reports *42*, 112696
July 25, 2023
https://doi.org/10.1016/j.celrep.2023.112696

CellPress

Cell Reports

CellPress
OPEN ACCESS

Article

Single-cell transcriptomics of NRAS-mutated melanoma transitioning to drug resistance reveals P2RX7 as an indicator of early drug response

Tijana Randic,[1] Stefano Magni,[2] Demetra Philippidou,[1] Christiane Margue,[1] Kamil Grzyb,[2] Jasmin Renate Preis,[1] Joanna Patrycja Wroblewska,[1] Petr V. Nazarov,[3,4] Michel Mittelbronn,[1,2,4,5] Katrin B.M. Frauenknecht,[5,6] Alexander Skupin,[2,4,7] and Stephanie Kreis[1,8,*]

[1]Department of Life Sciences and Medicine (DLSM), University of Luxembourg, 6, Avenue du Swing, 4367 Belvaux, Luxembourg
[2]Luxembourg Centre for Systems Biomedicine (LCSB), University of Luxembourg, 6, Avenue du Swing, 4367 Belvaux, Luxembourg
[3]Data Integration and Analysis Unit (DIA), Luxembourg Institute of Health, 1A-B, Rue Thomas Edison, 1445 Strassen, Luxembourg
[4]Department of Cancer Research (DoCR), Luxembourg Institute of Health (LIH), Luxembourg, 6A, Rue Nicolas-Ernest Barblé, 1210 Luxembourg, Luxembourg
[5]National Center of Pathology (NCP), Laboratoire National de Santé (LNS), 3555 Dudelange, Luxembourg
[6]Luxembourg Center of Neuropathology (LCNP), Dudelange, Luxembourg
[7]Department of Neuroscience, University of California San Diego, 9500 Gillman Drive, La Jolla, CA 92093, USA
[8]Lead contact
*Correspondence: stephanie.kreis@uni.lu
https://doi.org/10.1016/j.celrep.2023.112696

SUMMARY

Treatment options for patients with *NRAS*-mutant melanoma are limited and lack an efficient targeted drug combination that significantly increases overall and progression-free survival. In addition, targeted therapy success is hampered by the inevitable emergence of drug resistance. A thorough understanding of the molecular processes driving cancer cells' escape mechanisms is crucial to tailor more efficient follow-up therapies. We performed single-cell RNA sequencing of *NRAS*-mutant melanoma treated with MEK1/2 plus CDK4/6 inhibitors to decipher transcriptional transitions during the development of drug resistance. Cell lines resuming full proliferation (FACs [fast-adapting cells]) and cells that became senescent (SACs [slow-adapting cells]) over prolonged treatment were identified. The early drug response was characterized by transitional states involving increased ion signaling, driven by upregulation of the ATP-gated ion channel P2RX7. P2RX7 activation was associated with improved therapy responses and, in combination with targeted drugs, could contribute to the delayed onset of acquired resistance in *NRAS*-mutant melanoma.

INTRODUCTION

Melanoma is characterized by a high somatic mutational load and significant tumor heterogeneity and plasticity,[1] which hamper the development of "one for all" therapeutic approaches. Hyperactivation of the MAPK signaling pathway due to *BRAF* mutations occurs in ~50% of patients, while genetic alterations in the NRAS proto-oncogene GTPase ($NRAS^{mut}$) affect ~25% of all patients with melanoma, resulting in a highly aggressive malignancy with a growing incidence.[2] $NRAS^{mut}$ melanoma most frequently occurs in chronically sun-exposed, elderly patients, and to date, no efficient targeted therapy combinations have been approved for this melanoma subtype.[3] Current treatments for advanced $NRAS^{mut}$ patients include immunotherapy, radiation, chemotherapy, and MEK inhibition. However, not all patients tolerate immunotherapy, while in others it has no benefit.[4] Therefore, alternative therapeutic options, which can be administered before or after immunotherapy, are needed.[5] Given the constitutive activation of MAPK signal transduction in $NRAS^{mut}$ melanoma, the application of anti-MEK drugs (MEKi) is currently being tested in *in vitro* studies and clinical trials.[2,6,7] However, patient responses to MEKi are limited in time, with insufficient improvement over the chemotherapeutic drug dacarbazine.[7,8] To improve the therapeutic effect of MEKi, several clinical trials are currently testing the combination of MEKi with other targeted drugs (https://clinicaltrials.gov/).[9]

Disruption of cell-cycle progression with CDK4/6 inhibitors (CDK4/6is) has been described as a promising companion to MEKi in $NRAS^{mut}$ melanoma.[10,11] Yet, despite the initial benefit of MEKi and CDK4/6i co-therapy,[12] melanoma cells eventually learn to cope with the treatment. Described pathways for survival of MEKi/CDK4/6i treatment include upregulation of MAPK and PI3K signaling by activation of KRAS,[13] pre-existing $PIK3CA^{E545K}$ cell subpopulations,[14] and increased phopho-S6 levels.[11] Understanding the transitional processes conferring treatment resistance and assessing the transcriptional dynamics of cell states at the single-cell resolution provide a unique opportunity to define distinct cell populations that give rise to drug-resistant cell states.

By dissecting cellular heterogeneity, recent single-cell profiling of drug-exposed melanoma has provided deeper insights into transcriptional evolution toward drug resistance, especially in *BRAF*^{mut} melanoma.[15–18] However, a similar dataset was so far not available for treated *NRAS*^{mut} melanoma. In this study, we investigated cellular mechanisms that govern tolerance to combined MEKi/CDK4/6i by single-cell RNA sequencing (scRNA-seq) of four *NRAS*^{mut} melanoma cell lines over a prolonged treatment period until drug resistance was reached. In addition to previously described melanoma states,[15,16,19] our time-series setup (Figure 1A) allowed us to distinguish cell states involved in fast adaptive processes and delayed or slower responses to targeted treatment.

Our analysis revealed the involvement of the purinergic ATP-gated ion channel P2RX7 in early cell response to targeted therapy. However, controversy exists about whether P2RX7 should be inhibited or activated, and this likely depends on the type and stage of the tumor as well as the type of therapy that is applied.[20] Here, we show that high levels of P2RX7 are associated with initial *NRAS*^{mut} melanoma treatment response, whereas hyperactivation of P2RX7 in combination with MEKi/CDK4/6i delays the onset of acquired drug resistance.

RESULTS

Characterization of *NRAS*^{mut} melanoma cell line responses under MEK/CDK4/6 inhibition

To investigate the development of drug resistance in *NRAS*-mutation-based melanoma, we used three commercial *NRAS*^{mut} melanoma cell lines (IPC298, SKMel30, and MelJuso) and one primary line (M20) established from an *NRAS*^{mut} patient. For these cell lines, we first established optimal concentrations of MEKis (binimetinib, cobimetinib, and trametinib) and CDK4/6is (palbociclib and ribociclib) (Figure S1) and pairwise combinations of two of them (binimetinib and palbociclib) (Figure S2). As expected, the combination matrix indicated a decreasing inhibition over time, suggesting drug resistance. For the subsequent time-series experiments, the averaged cell-line-specific IC_{50} values of binimetinib (27 nM [M20], 110 nM [MelJuso], 35 nM [SKMel30], and 16 nM [IPC298]) and 1 μM palbociclib for all cell lines were used. The time points for single-cell transcriptomic measurements were chosen to represent both early and late transcriptional adaptations to treatment (1, 4, and 33 days; Figure 1A), and untreated samples (0 day) were used as a control condition.

Interestingly, IPC298 and SKMel30 cells were proliferating already after 33 days of treatment, whereas M20 and MelJuso cells did not resume proliferation during this period (Figures 1A and 1B). Based on this difference, we will refer to the IPC298 and SKMel30 lines as fast-adapting cells (FACs) and to the MelJuso and M20 lines as slow-adapting cells (SACs). Reactivation of the MAPK and PI3K pathways in FAC lines (Figure 1B) with rapid re-entry into the cell cycle (Figure 1C) was detected once they became adapted to combined drugs. Moreover, partial restoration of protein expression and phosphorylation of the CDK4/6 downstream target RB1 was detected in long-term treated FACs (Figure 1B), whereas complete pRB rebound was observed under a MEKi-therapeutic regimen (Figure S3). As expected, FACs resumed cellular proliferation under MEKi or CDK4/6i monotherapy within 33 days (Figure S4A).

Next, we observed that combined therapy affected the levels of RB and pRB and prevented signal transduction through the MAPK and PI3K pathways even after 33 days of drug exposure in SAC lines (Figure 1B). Monotherapeutic effects of MEKi in SACs were sustained over time, while CDK4/6i treatment was tolerated, as shown by a significant increase in pRB levels (Figure S3). SACs reacted to treatment with cell-cycle arrest indicated by reduced Ki-67 staining (Figure 1C) and became fully senescent upon MEKi and CDK4/6i prolonged exposure (Figure 1D). In contrast to the combined treatment, extended exposure to monotherapy induced neither cell-cycle arrest (Figure S4A) nor senescence, with the exception of long-term CDK4/6i treatment of M20 cells (Figure S4B). Single or combined MEK/CDK4/6 inhibition induced cell-cycle arrest rather than apoptosis (Figures 1E and S4C). Taken together, MEKi/CDK4/6i evoked diverse cell survival programs, suggesting that patients also might rapidly relapse under such a treatment combination.

Single-cell transcriptomic profiling of MEKi/CDK4/6i-treated *NRAS*^{mut} melanoma cells

To profile transcriptional transitions from a drug-sensitive to a resistant phenotype, we isolated and sequenced ~48,000 cells from all four cell lines at four different time points (0, 1, 4, and 33 days). After quality control and filtering (Figure S5), the scRNA-seq data of ~15,000 cells were integrated and batch-corrected based on the cell line origin (Figure 1F).

First, all cell lines and time points were considered together. Interestingly, FACs that re-entered proliferation after 33 days clustered together with untreated cells, predominantly found in the G2M/S phase (Figure 1F). Treated SACs, in contrast, cluster in G1 at all time points, illustrating a rapid induction of an enduring cytostatic program. By employing Slingshot pseudotime analysis,[21] pseudotime trajectories were reconstructed by ordering cells based on minimal differences in their transcriptomes. Indeed, after a long treatment, FACs moved back toward the initial untreated cell state, while SACs were still arrested in the G1 phase (Figure 1G).

Next, we investigated gene signatures previously related to melanoma heterogeneity and resistance to targeted therapy (Table S1).[15,16,22] MITF high/AXL low, mesenchymal, and pigmentation signatures were observed in early *NRAS*^{mut} melanoma-treated states (1 and 4 days). Cell populations corresponding to the non-proliferating SACs expressed genes characteristic of MITF low/AXL high, neural, invasive, migratory, and epithelial-mesenchymal transition (EMT)-like phenotypes (Figure S6A), previously described in treated *BRAF*^{mut} melanoma.[15,22] The expression of marker genes indicative of resistance to MEKi and/or CDK4/6i in *NRAS*^{mut} melanoma was analyzed across time points (Figure S6B). This analysis revealed increased gene levels of cyclin D1 (*CCND1*), in agreement with previous findings on *NRAS*^{mut} melanoma drug resistance.[11,13,14] As expected, the mRNA levels of cell-cycle-related kinases (*CDK1*, *CDK2*) were reactivated in 33-days-treated FACs, while they remained inhibited in senescent SACs. In contrast to prior findings where MEKi was combined with CDK4/6i,[11,13,14] we detected no increase in *mTOR* and *RBS6KB1* in long-term drug-exposed cells

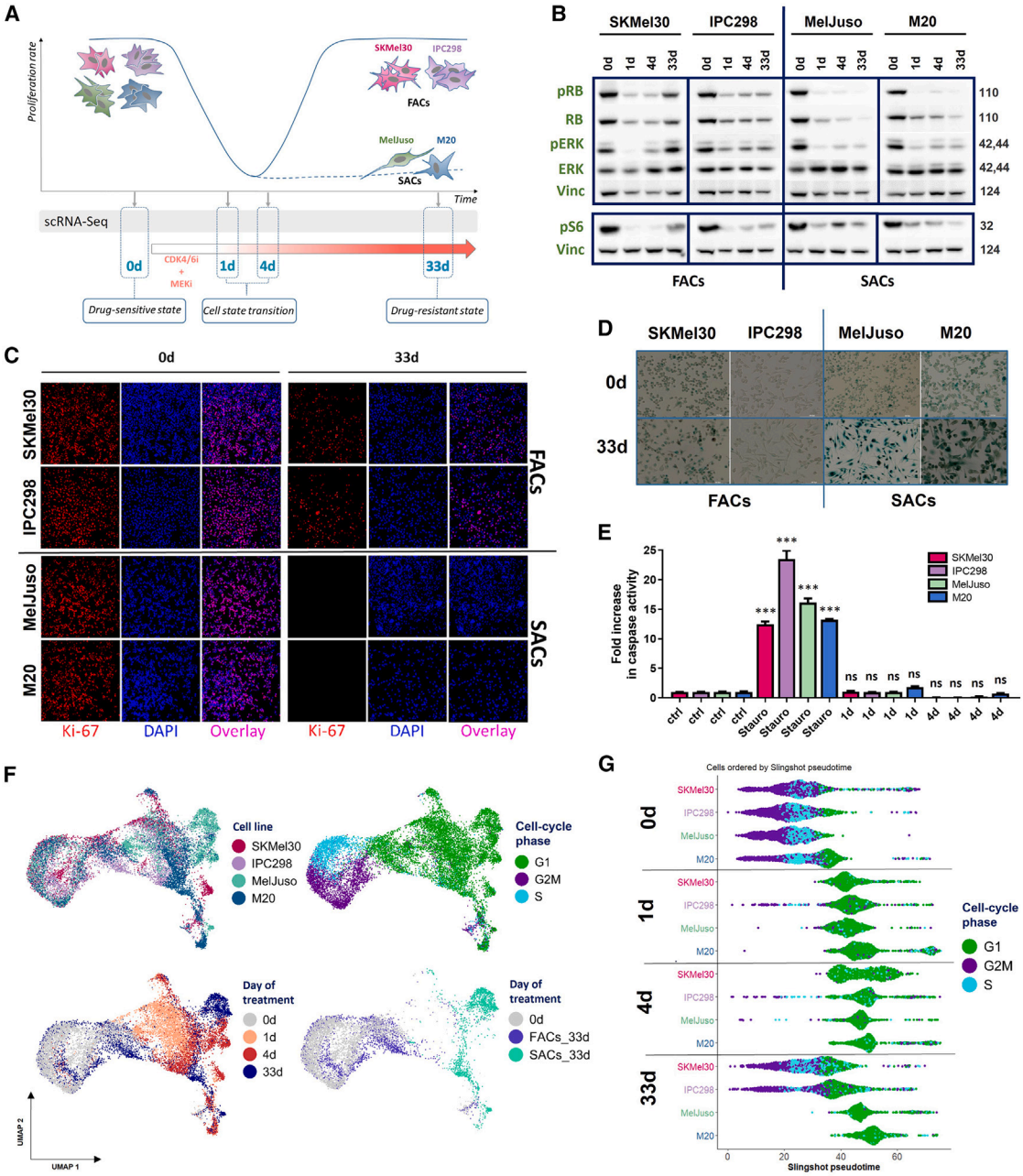

Figure 1. Phenotypic characterization of cell lines: Combined therapy induces a switch to both fast (FACs) and slow (SACs) adaptive states

(A) Schematic representation of *NRAS*^{mut} melanoma cell response upon treatment with MEK1/2 and CDK4/6 inhibitors.

(B) Effects of MEK1/2i and CDK4/6i combined therapy on drug target downstream signaling. Phosphorylated and total levels of RB, ERK, and S6 were assessed in untreated (0 day) and treated (1 day, 4 days, and 33 days) melanoma cell lines by immunoblotting. Vinculin was used to confirm equivalent loading. Molecular weights are shown in kilodaltons.

(C) Cell proliferative activity determined with Ki-67 (red), and DAPI (blue) staining was used to mark nuclei.

(D) Senescence β-galactosidase (SA-β-gal) activity was confirmed in non-proliferating SACs (MelJuso and M20).

(E) The activity of caspase-3 upon MEKi/CDK4/6i treatment was measured by an AC-DEVD-AFC apoptosis assay, revealing the absence of apoptosis in response to drug exposure for 1 and 4 days. Plotted data represent the mean ± SD obtained from three biological replicates. One-way ANOVA, followed by multiple comparisons test, was utilized to calculate p values (ns, not significant; ***$p \leq 0.001$).

(F) Treated *NRAS*^{mut} melanoma cells exhibit heterogeneous cell responses. The four presented graphs represent integrated data of cell lines included in the study (top left), cell-cycle phase (top right), and days of cell treatment (bottom), visualized by UMAP dimensionality reduction.

(G) Slingshot single-cell pseudotemporal ordering based on the overall transcriptional program, colored by cell-cycle position, shows transcriptional dynamics corresponding to cell-cycle restart.

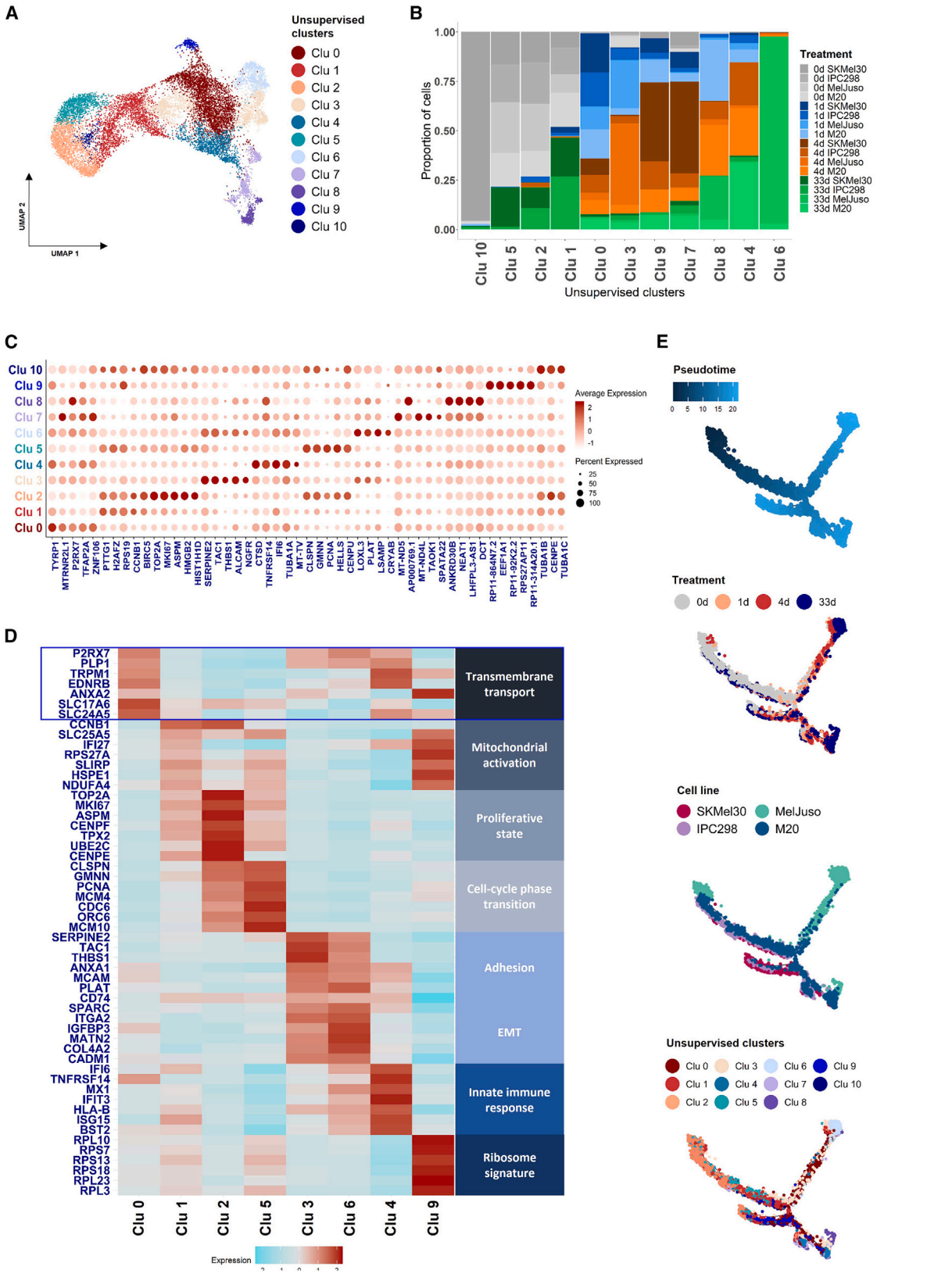

(legend on next page)

(Figure S6B). Similar to Hayes et al.,[13] we found decreased RPS6 gene and pS6 levels in treated SACs, while S6 gene expression and protein pS6 levels were increased in 33-days-treated FAC lines (Figures 1B and S6B).

Treated *NRAS*^{mut} melanoma cells exhibit heterogeneous transcriptional responses

Considering the two general drug response types of FACs and SACs, we hypothesized that combined MEKi/CDK4/6i therapy may induce specific *NRAS*^{mut} melanoma subpopulations with distinct fate trajectories, ultimately leading to tumor growth advantages. Thus, we performed unsupervised clustering on all cell lines, regardless of treatment duration. Eleven clusters were identified (Figure 2A), and the cell line composition of each cluster was assessed and grouped by content similarity (Figure 2B). Treated cells of all four cell lines and time points group in clusters 0, 4, 6, and 8, which contain almost no untreated cells, while cluster 10 is made up almost entirely of untreated SKMel30 cells (Figure 2B). Clusters 7 and 9 mostly consist of intermediate (1 and 4 days) time points of SKMel30, IPC298, and M20 lines, while cluster 3 is predominantly formed by MelJuso early treated cells. Upon long-term drug exposure, treated FACs congregate together with untreated states (0 day) in clusters 1, 2, and 5 (Figure 2B), which contain hardly any cells from the intermediate time points. Long-term treated MelJuso and M20 cells are abundant within clusters 6, 8, and 4.

Next, we computed differentially expressed genes (DEGs) of each cluster compared with all others (Figure 2C). Among the top DEGs expressed within cluster 0, which is mostly composed of intermediate time points, are tyrosinase-related protein 1 (*TYRP1*), the antiapoptotic factor *MTRNR2L1*, and *P2RX7*. Meanwhile, elevated levels of the IFI6 gene are seen in cluster 4, containing cells from all four lines at 4 and 33 days of treatment. De-differentiation markers *ALCAM* and *NGFR*[23] are among the top DEGs in cluster 3, which mostly contains MelJuso cells from intermediate time points (Figure 2C and Table S2). Based on DEGs between clusters, we further assessed which pathways are enriched in each cluster (Figure 2D and Table S2). "Transmembrane transport" emerged as the most relevant term in cluster 0. Several genes involved in interferon signaling (e.g., *IFI6*, *IFI27*, *IFIT3*, and *MX1*) were upregulated under treatment with peak expression levels at 4 and 33 days (clusters 4 and 6; Figures 2D and Table S2). As expected, the expression levels of genes involved in the targeted signaling pathways (MAPK and cell cycle), such as *E2F2*, *PCNA*, and *TOP2A*, strongly decrease under treatment, in contrast to clusters 2 and 5, which are enriched in genes involved in proliferation. Next, we checked DEGs in each cell line separately. Upon removal of a potential bias introduced by cell-cycle genes, key signatures in each time point did not change significantly, suggesting robust annotations (Table S3).

To compare the dynamics of gene expression between time points, we mapped cells along trajectories of transcriptional changes (Figures 2E and S7) using Monocle's pseudotime.[24] Multiple branches corresponding to various trajectories are followed by cells with distinct transcriptional programs. Untreated cells are mostly distributed along the upper left branch, while intermediate time points are found along all other branches. Clusters 1, 2, and 5, containing both 0 and 33 days FACs, appear on the upper left branch together with cluster 10. The upper right branch mostly consists of 33-days-treated SACs (cluster 6) and treated MelJuso cells at all time points (Figures 2E and S7A). In addition, treated IPC298, M20, and SKMel30 cells group along lower branches corresponding to intermediate pseudotimes (Figure S7A). This analysis confirms that transcriptional states of SACs at 33 days are diverse (multiple branches) but distinct from the untreated state, whereas FACs' transcriptional state at 33 days reverts back to the untreated state. This becomes even more pronounced when analyzing cellular distributions in one-dimensional (1D) pseudotime (Figure S7B). By merging different branches corresponding to the same pseudotime and plotting the corresponding density of cells, we observed that distributions from untreated and long-term treated samples have almost no overlap for SAC lines (Figure S7B, right column, first and third rows). For MelJuso in particular, these two distributions lie at the opposite extremes of pseudotime. In contrast, in FACs there is considerable overlap between the untreated and the treated cell distributions (Figure S7B, left column, first and third rows).

Targeted therapy triggers ion transport in FACs and SACs and initiates immune response programs in FACs

To scrutinize the effects of early drug exposure and analyze if *NRAS*^{mut} subpopulations exist that either intrinsically resist therapy or rapidly acquire traits that allow them to escape drug pressure, we assessed transcriptional programs of FACs and SACs separately at each time point. In Figure 3, we combined uniform manifold approximation and projection (UMAP) dimensionality reduction and unsupervised clustering to characterize transitions of the cell populations between transcriptional states over time, with heatmaps showing the top 3 DEGs per cluster. Gene set enrichment analysis (GSEA) was used to establish the most enriched signatures for each cluster (Table S4), which are highlighted in Figure 3. Already after 1 day of treatment, both SACs and FACs responded with considerable adaptations of gene expression, especially in genes involved in ion transmembrane transport and cell-cell signaling, e.g., *P2RX7*, *PLP1*,

Figure 2. Unsupervised clustering reveals cell populations across time points

(A) Eleven clusters of cells were obtained when performing unsupervised clustering of integrated data from all cell lines and treatment durations.

(B) Relative abundance of cells for each time point and cell line, within each cluster.

(C) Top differentially expressed genes (DEGs) between the clusters obtained from all treatment phases and cell lines together. The size of the circles indicates the percentage of cells in each cluster that express a given gene.

(D) Heatmap of the relative average expression of the DEGs corresponding to biologically relevant enriched pathways for selected clusters, identified by the log-fold change in cells in one cluster compared with all other cells (with adjusted $p < 0.05$).

(E) Pseudotemporal ordering of cells from all cell lines and time points, arising from the temporal dynamics of transcriptional changes and depicting the phenotype switch toward cell static/proliferative states; cells are colored by their pseudotime value (first subpanel), time point of treatment (second), cell line (third), and the cluster they belong to (fourth).

S100B, and *SOX4* (Figures 3A, 3B, and S8 and Table S4). Interestingly, although the "transmembrane transport-related state" (subsequently referred to as "trans-state") is predominant in FACs after 1 day of treatment (Figure 3A, UMAP plots), most FACs switch to an "immune-like state" over time (4 and 33 days), reminiscent of an antiviral immune response, in which IFI6 displays the highest upregulation (Figures 3A and S8A and Table S4). In contrast to FACs, in which the trans-state is replaced by an immune-like state, SACs retain high expression of genes involved in the trans-state, such as *P2RX7* and *SOX4*, regardless of treatment duration (Figure S8B). Next to the trans-state, upon 1 day of treatment, SACs also switch into a cell subpopulation enriched in cell migration ("migratory state"; cluster 4) (Figure 3B). Cells with similar signature were also found after 4 days (cluster 3) of therapy. *FN1*, *PLP1*, *SEMA3B*, *SEMA3C*, and *LOXL2* are among the top DEGs within migration-enriched clusters (Table S4). In addition, high expression of *NGFR* and *THBS1*, previously described in the neural crest stem cell (NCSC)-like state,[15] is found in this cluster. Trans- and migratory state also have a certain number of shared enriched pathways (Table S4). Thus, they most likely represent the two extremes of transcriptional programs of the same cell population rather than two mutually exclusive populations. After 33 days of therapy the migratory state does not appear as a separate cluster, whereas the cluster enriched in adhesion emerges as an independent state (Figures 3B and Table S4).

Compared with gene signatures previously described in melanoma plasticity and drug resistance,[19,25–27] a subset of cells highly expressing pigmentation markers is found within the trans-like cluster in FACs and SACs (Figure S9). Furthermore, cells highly expressing pigmentation-related genes also persist over time in the FACs immune-like state. Cells with an invasive/migratory phenotype (reminiscent of a mesenchymal-like state) are found in both untreated and MEKi/CDK4/6i-treated FAC lines (Figures S9A–S9C). Similarly, cells with the previously described mesenchymal-like phenotype are also found within SAC untreated and treated trans-like states (Figures S9D–S9F). Notably, cells expressing NCSC markers, in particular neural crest cells,[15,25] are not detected in FAC lines (Figures S9A–S9C), while they are present in SAC trans- and migratory-like states (Figures S9D–S9F).

Next, we identified a cluster that involves untreated and treated cells, appearing in both FACs and SACs, with similar top DEGs. We termed this cluster "intrinsically resistant (inres)-state" due to its assumed intrinsic potential to evade therapeutic pressure and retain a similar transcriptional signature (Figures 3A and 3B and Table S4). The inres-state is characterized by high expression of the long non-coding RNAs *MALAT1* and *NEAT1*, previously described in metastatic/invasive melanoma,[28–30] as well as AP000769.1 and *GABPB1-AS1* (Figures 3A, 3B, and S8 and Table S4). These genes might therefore represent markers for intrinsic drug resistance.

To predict gene-regulatory networks and regulon activity in different melanoma subpopulations, we applied the single-cell gene-regulatory network inference and clustering (SCENIC) method (Figure 4).[31] SCENIC revealed that upon 1 day of therapy, DEGs in the FACs trans-state are regulated by transcription factors (TFs) SOX4, JUN, and MITF, the activity of which has been previously associated with both mesenchymal-like (JUN and SOX4) and melanocytic (MITF) states.[19,27,32] The immune-like state (appearing after 4 days in FACs) also displays the activity of the interferon-related TFs STAT1, STAT2, IRF7, JUND, and MXD4 (Figure 4A and Table S5). In 1- and 4-days-treated SACs, the TFs ETS1, SOX4, STAT2, and JUN display increased activity in the trans-state (Clu 0) (Figure 4B and Table S5). POU3F2, CREB5, and NFATC2 are among regulons that are specific to the SAC migratory state after 1 day (Clu 4) and 4 days (Clu 3) of treatment, whereas MITF activity is not detected. Last, many regulons are found in the inres-state in both SACs and FACs, where among the shared ones are IRF3, SP1, ZNF274, and STAT3 (Figures 4A and 4B and Table S5).

Overall, we identified transcriptional states characteristic of transport signaling at 1 day of treatment in both FACs and SACs, mostly driven by ETS1, SOX4, and JUN, as well as activated immune response signatures taking over the transcriptional landscape in 4-days-treated FACs.

Transcriptional changes in treated *NRAS*^{mut} melanoma reveal switches toward senescent-like or proliferative phenotypes

Upon analysis of genes that may drive FACs' accelerated ability to re-enter the cell cycle compared with SACs, we confirmed programs involved in ion transport and migration (Figures 5A, 5B, and S10A), while a decrease in expression levels of genes involved in proliferation characterized 33-days-treated SACs. As seen before, genes that are highly expressed in 33 day FACs are enriched in immune response programs. Yet, differences between 0- and 33-days-treated FACs are not as striking as in the case of SACs.

Considering that the trans-state occurs in early drug-exposed FACs and at all time points in SACs, we speculated that SAC lines would eventually overcome the state of senescence and re-enter the cell cycle. Indeed, we observed that, after 3 months of therapy, both MelJuso and M20 eventually resisted the combined MEKi/CDK4/6i, escaped cell-cycle arrest, and resumed proliferation (Figures 5C and S10B). These findings are supported by augmented levels of pRB, diminished activity of β-gal (Figures 5D and 5E), and higher binimetinib IC_{50} values in comparison with sensitive cells (Figures S1 and S10C).

To assess which genes are associated with delayed drug resistance, we plotted the top DEGs that are shared between FAC intermediate time points and all treated SAC time points (Figure 5F). This intersection includes *P2RX7*, *SOX4*, *JUN*, *ADAM23*, *PLP1*, and *COL4A3BP*, indicating their involvement in the maintenance of a senescent, non-proliferative cell state. Further, *IFI6* is significantly expressed in FACs (1, 4, and 33 days) and only in 33 days SACs and may contribute to an eventual switch toward the on-drug proliferative state. DEGs shared between all treated cells are *S100B*, *TYRP1*, and *TUBA1A* and may implicate transcriptional activities that persist over time and support a drug-resistant phenotype.

Next, we compared correlations and shared DEGs between treated FAC and SAC lines in our study and recently published data from Rambow et al.[15] representing different phases of *BRAF*^{mut} melanoma treatment, where phase 1 describes early drug response; phase 2, "minimal residual disease" (MRD); and phase 3, completely drug-resistant melanoma cells.[15] While

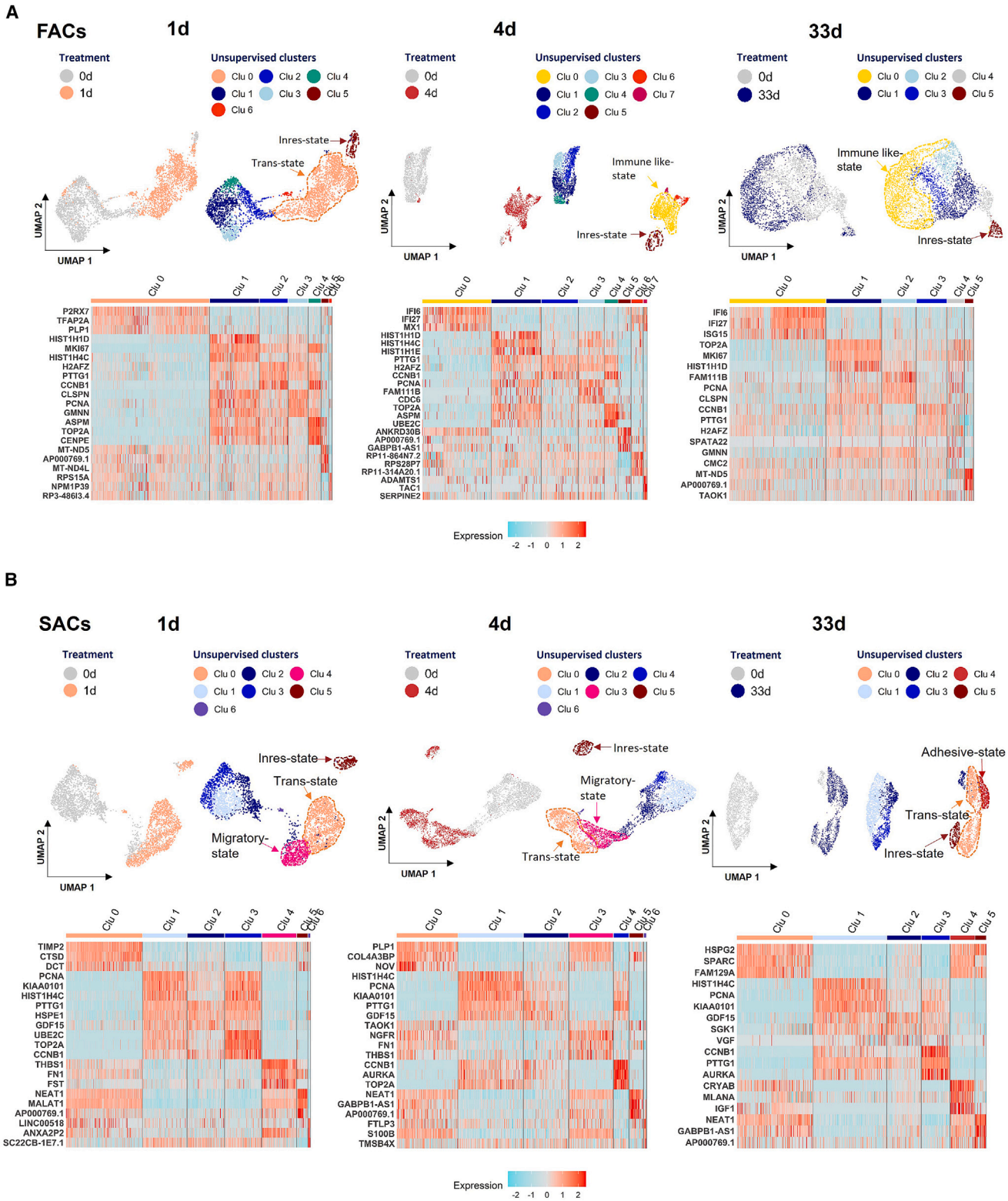

Figure 3. Discrete effects of MEK1/2i and CDK4/6i combined treatment in SACs and FACs at each time point separately

UMAP plots of the different treatment phases in FACs (A) and SACs (B), each treated time point compared with untreated cells, and corresponding unsupervised clustering. Heatmaps depict the top three DEGs in each cluster.

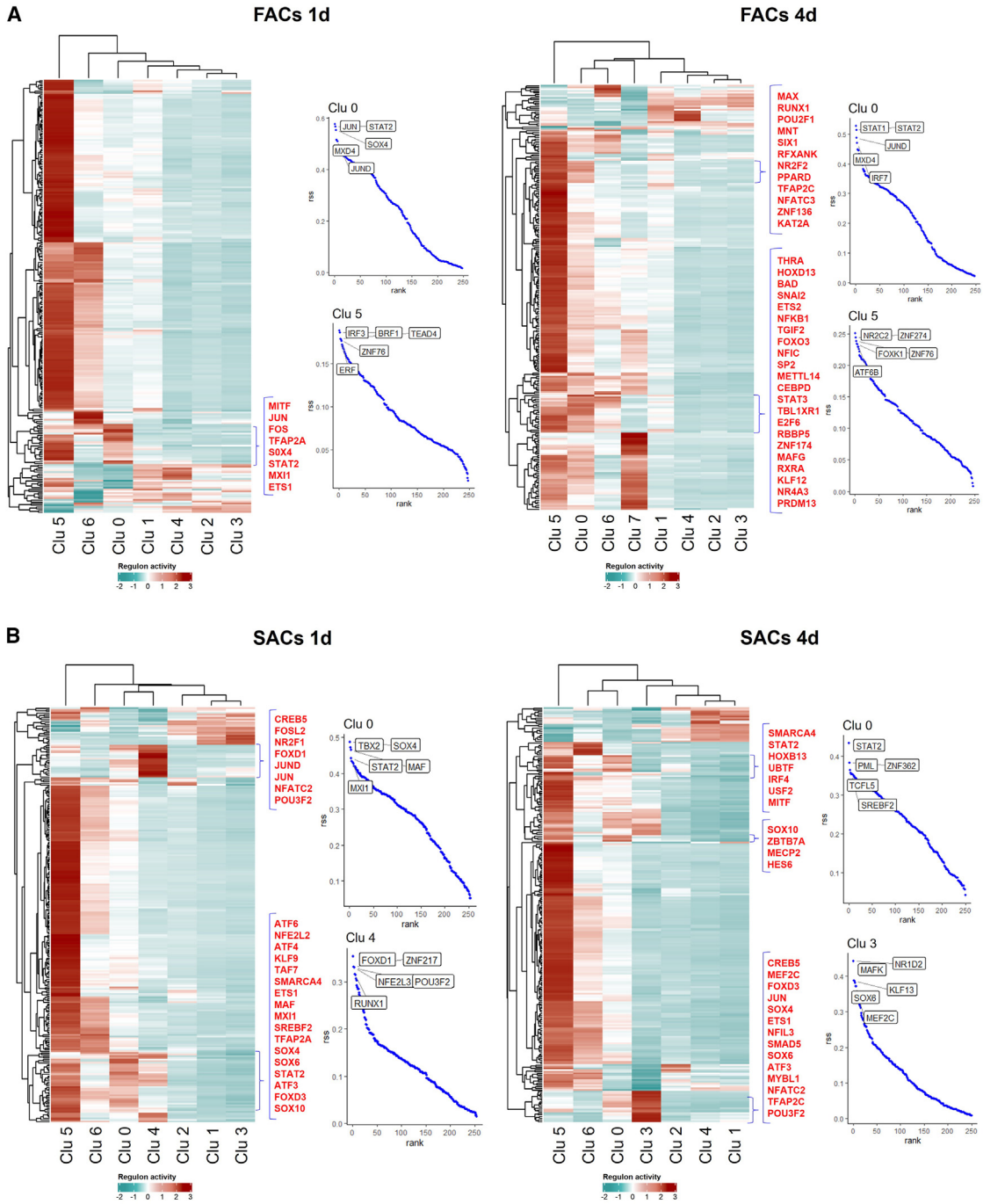

Figure 4. SCENIC analysis reveals transcriptional factors and their target genes in short-term treated *NRAS*^{mut} melanoma cells

(A and B) Heatmaps showing average regulon activities (scored by AUCell) in each cluster upon 1 and 4 days of treatment in FACs (A) and SACs (B). The indicated regulons represent the highly active ones in the trans-state (Clu 0: 1 day FACs, 1 day SACs, and 4 days SACs), as well as the migratory state in SACs after 1 day (Clu 4) and 4 days (Clu 3) of treatment. Plots represent treated cluster-specific regulators calculated by regulon specificity score (rss), where the top 5 regulons are shown.

all treated SACs (1, 4, and 33 days) and early treated FACs (1 and 4 days) mostly correlate with phases 1 and 2, drug-resistant 33-days-treated FACs resemble the profiles of drug-resistant phase 3 (Figure S11A). Interestingly, *TYRP1* is found among genes expressed at all time points of treatment in our and Rambow et al.'s[15] melanoma datasets (Figures S11B and S11C). *SOX4*, *PLP1*, *TFAP2A*, and *CD36* are among the commonly significant DEGs between intermediate time points of SACs and

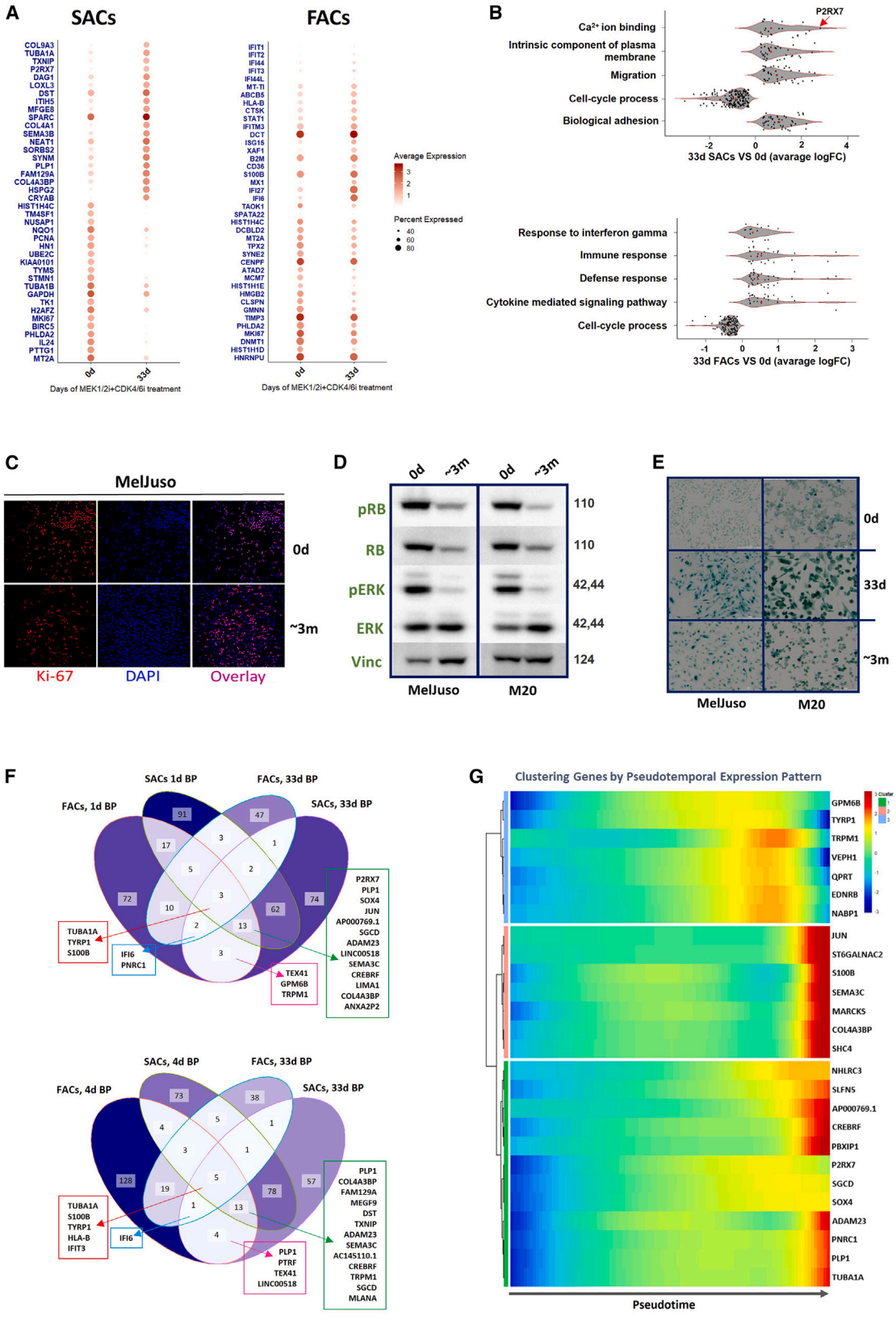

(legend on next page)

FACs and phases 1 and 2. Resistant melanoma cells in phase 3 share markers implicated in immune states (IFI27 and MX1) with our long-term treated FACs (Figure S11B), while IFIT3 is highly expressed at all time points of SACs and resistant melanoma cells in phase 3 (Figure S11C).

Gene clustering based on gene expression across pseudotime was performed by Monocle (Figure 5G), considering a selection of genes shared among distinct phenotypes. We plotted the dynamics of expression of these genes and visualized their pseudotime dependency, i.e., how their expression varies across pseudotime. From the mapping in Figure 2E, we can identify early pseudotime values corresponding to untreated and 33-days-treated FACs. These values correspond to those of the upper left branch of the images in Figure 2E (dark blue in the top image) and those on the left of the pseudotime axis in Figure 5G. Late pseudotime values (pale blue in the top image of Figure 2E and right side of the horizontal axis of Figure 5G) matched to 33 days SAC time points, with all treated 1 and 4 days cells corresponding mainly to intermediate values (the central part of Figure 5G). Here, *P2RX7* and *SOX4* are highly expressed at intermediate and late pseudotime values, while *JUN* is exclusively highly expressed at late pseudotime values.

P2RX7 expression levels mark responses to targeted treatment in *NRAS*^{mut} melanoma

Since we observed in all cell lines the trans-state with high P2RX7 levels after early drug exposure and especially after 33 days of treatment (Figures 3A and 5A), we assessed if the expression of P2RX7 is associated with the proliferative status of *NRAS*^{mut} melanoma cells following single/combined treatment. We confirmed that P2RX7 mRNA and protein levels were elevated upon early treatment involving MEKi in all cell lines (Figures 6A and 6B). The antibody used here recognizes a protein of around 78 kDa, which corresponds to the predicted molecular weight of the full-length splice variant P2RX7A. While we focus here on the P2RX7A isoform, we also detected a similar upregulation of the shorter isoform, P2RX7B, upon inhibition of MEK and CDK4/6 in four of five tested *NRAS*^{mut} melanoma cell lines (data not shown).

Upon resuming proliferation (Figures 1C and S4A), P2RX7 protein levels decreased in treated FACs (Figure 6A). Likewise, when after ~3 months treated SACs eventually restored proliferation, P2RX7 protein levels dropped to control levels (Figure 6A), suggesting that higher P2RX7 levels are indeed indicative of the on-drugs *NRAS*^{mut} melanoma proliferative status. This is supported by decreased levels of P2RX7 protein and mRNA in 33 days-treated-SAC lines, which re-enter the cell cycle after monotherapy, in contrast to non-proliferating SACs exposed to 33 days of combined treatment (Figures 6A and 6B).

Next, we analyzed if elevated levels of P2RX7 in *NRAS*^{mut} melanoma cells undergoing cytostatic growth arrest might also be accompanied by metabolic reprogramming. P2RX7 was stimulated with its non-selective agonist 2′(3′)-O-(4-benzoylbenzoyl) adenosine-5′-triphosphate (BzATP), which in previous studies was demonstrated to be ~10–30 times more potent in P2RX7 activation compared with normal ATP,[33,34] followed by Seahorse quantitative kinetic profiling of mitochondrial and glycolytic ATP production rates. Combined treatment reduced overall ATP production, confirming the cytostatic effect of MEKi/CDK4/6i at 1 and 4 days of treatment. Conversely, activation of P2RX7 channels by BzATP restored the produced glyco- and mitoATP to untreated control levels (Figure 6C). Interestingly, in SACs (MelJuso), only glycoATP levels were affected, indicating a switch to oxidative phosphorylation (OXPHOS) metabolism. Along these lines, tonic P2RX7 stimulation has previously been shown to enhance mitochondrial potential and OXPHOS efficiency, while P2RX7 overstimulation has been related to a decreased mitochondrial potential resulting in cell death.[35] Extracellular ATP levels strongly increased after 4 days of treatment, concomitant with decreased ATP consumption rates (Figures S12A and S12B).

Together, these results indicate that high levels of active P2RX7 could be a useful marker for a general response to treatment, as levels drop in cells that have become resistant to therapy. This notion is supported by the fact that high expression of P2RX7 is associated with significantly longer overall and progression-free survival in *NRAS*^{mut} melanoma patients (Figure S13A). Remarkably, this beneficial effect is not seen in *BRAF*^{mut} melanoma patients (Figure S13B), indicating a possible connection between *P2RX7*-induced metabolic rewiring and *NRAS* mutational status. Furthermore, heterogeneous P2RX7 expression was found in tumor tissues of a small cohort of patients with melanoma (harboring *NRAS*^{mut} [5 patients] or *BRAF*^{mut} [5 patients] or being *NRAS*-/*BRAF* wild type [4 patients]) by using an antibody targeting the N terminus of P2RX7, but also across melanoma cell lines (Figures S14A–S14E and Table S6). Overall, *NRAS*^{mut} melanoma appeared to have higher P2RX7 expression, but this finding requires confirmation in a larger cohort including treatment-naive and resistant patient samples. Therefore, next to the detected levels of P2RX7 in *NRAS*^{mut} melanoma that are enhanced by

Figure 5. Dynamic changes result in a cellular transition to a melanoma proliferative drug-resistant state

(A) DEGs between integrated (0 day) and 33-days-treated integrated SACs (left) and FACs (right).

(B) Gene set enrichment analysis (GSEA) shows the top enrichment of gene sets in 33-days-treated versus untreated cells. Each dot represents a log2-fold change in one of the genes describing a given gene signature.

(C) Ki-67 activity in MelJuso (SAC) upon very-long-term drug exposure of ~3 months.

(D) Upon prolonged treatment (~3 months), SACs also re-enter cell-cycle progression, as shown by phosphorylated RB and ERK levels. Vinculin levels were used as a western blot loading control. Molecular weights are shown in kilodaltons.

(E) Upon prolonged (~3 months) treatment, SA-β-gal activity diminished in both SAC lines, compared with 33 days treatment.

(F) Common genes found among top DEGs between 1 day (top) or 4 days (bottom) and 33 days of treatment. Cell lines were grouped at each time point based on proliferative cell fate upon long-term therapy exposure (SAC and FAC).

(G) Expression heatmap showing kinetic trends of common DEGs shared between early treated FACs and long-term drug-exposed (33 days) SACs plotted in pseudotime, with columns representing pseudotime points. The rainbow color scale indicates gene expression, with red being very high and blue being very low. Genes that co-vary similarly across pseudotime cluster together.

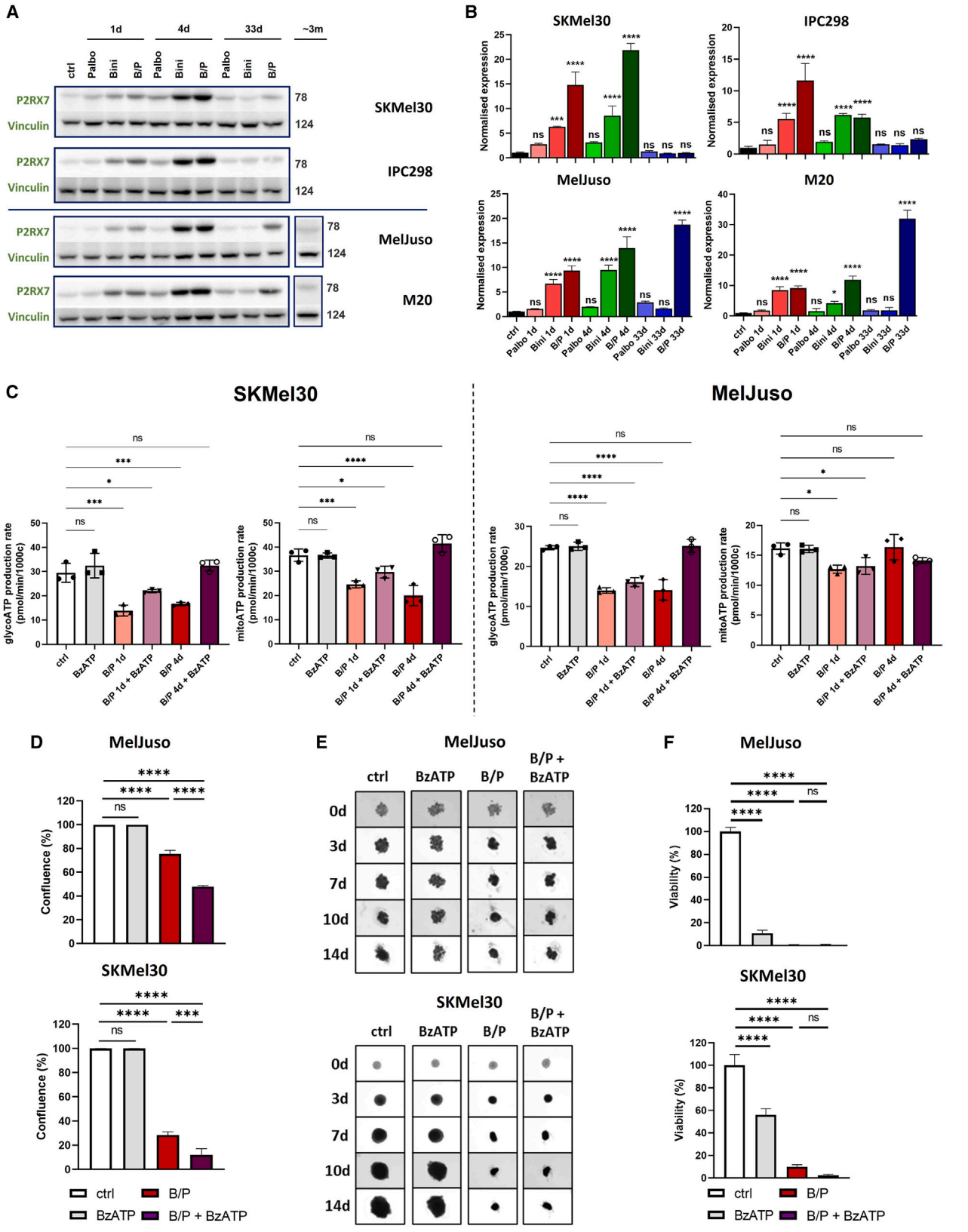

(legend on next page)

MEK/CDK4/6 inhibition, we hypothesize that an additional P2RX7 activation might support the cytostatic drug effect. Indeed, simultaneous exposure to BzATP and combined MEKi/CDK4/6i treatment significantly decreased growth in both *NRAS*^{mut} melanoma FAC (SKMel30) and SAC (MelJuso) lines grown in 2D (Figures 6D and S15), as well as in 3D spheroid models (Figures 6E, 6F, and S16). Interestingly, combined MEKi and CDK4/6i treatment was much more potent in 3D models compared with regular 2D tissue culture, killing most cells after 14 days. Therefore, we could not observe an augmented tumoricidal effect of P2RX7 stimulation (Figures 6E, 6F, S16A, and S16B).

Mechanistically, P2RX7 is known to mediate Ca^{2+} influx, which results in increased production of reactive oxygen species (ROS).[36–38] Consequently, we examined if elevated ROS levels mediate the cytotoxic effects of P2RX7 stimulation. Indeed, high intracellular ROS levels were induced by CDK4/6 and MEK co-inhibition within 1 and 4 days (Figures 7A and 7B). Simultaneous P2RX7 activation with BzATP further increased ROS levels, and this effect was abolished when P2RX7 was silenced by siRNA (Figure 7B). Similarly, inhibition of P2RX7 by a specific antagonist, A-740003, enhanced the growth of MEKi/CDK4/6i/BzATP-exposed SACs (MelJuso) (Figure 7C), but also diminished ROS production induced by P2RX7 stimulation (Figure 7D). P2RX7 inhibition did not affect the cellular growth of drug-naive and treated *NRAS*^{mut} melanoma cell lines (Figure S17). Notably, BzATP did not have an impact on ROS production in FACs (SKMel30), probably due to their phenotypic properties to rapidly resist therapeutic effects (Figure S18). Overall, activation of P2RX7 channels alongside targeted treatment led to higher levels of ROS in SACs (Figure 7B), which could support the induction of cell death in treated melanoma cells.

DISCUSSION

Tumor heterogeneity and plasticity prevent sustained responses to targeted therapies and allow cancer cells to eventually adapt to known treatments.[39,40] Melanoma, with its extremely high numbers of somatic mutations,[2] is notorious for its ability to escape cytostatic or immune-modulating treatments, and clonal selection of resistant cells following tumor therapy is a commonly occurring phenomenon.[40]

Diverse molecular signatures and functional profiles of *BRAF*^{mut} and *NRAS*^{mut} melanoma cells have been described, which can explain dynamic cellular responses, sensitivity, or resistance to drugs.[41,42] Previously, single-cell profiling of treated *BRAF*^{mut} melanoma has identified different phenotypic states, including NCSC-like, pigmented, invasive, starved, and stress-like cellular states.[15,16] Rambow and colleagues coined the term "minimal residual disease," which describes melanoma drug-tolerant cell states, in which both expansion of pre-existing cell populations and *de novo* transcriptional reprogramming may occur under pharmacological perturbation.[15,43] Detecting early resistance would be clinically beneficial, as it would allow switching treatment regimens before patients deteriorate further.[42] Much less information is available on the plasticity of *NRAS*^{mut} melanoma. Thus, we conducted a single-cell study on *NRAS*^{mut} melanoma transcriptional states at different time points (0, 1, 4, and 33 days) under MEKi/CDK4/6i treatment, allowing us to characterize both intrinsically and *de novo* drug-resistant *NRAS*^{mut} cell subpopulations.

Immediate responses to treatment revealed a melanoma trans-state, which is highly enriched in genes involved in ion transmembrane transport, particularly Ca^{2+} transport, such as *P2RX7*, *S100B*, and *PLP2*. Moreover, a striking interferon gene signature was detected after 4 days in FACs, which might allow cells to rapidly respond to drug-induced stress.[44] SAC lines were undergoing longer cell-cycle arrest in comparison to FACs and only after 3 months of treatment switched toward a proliferative phenotype. Therefore, before transitioning into a differentiated (proliferative) melanoma state enriched in a signature that is characterized by interferon-induced genes, all MEKi/CDK4/6i-treated cells went through the above-mentioned trans-state. Next to the trans-state, we found both EMT and migration signatures in treated SAC lines. While elevated MITF expression was found in FACs, together with other TFs related to the trans-state (SOX4 and JUN), in the SAC migratory state, we observed POU3F2 regulon activity, whereas MITF activity was diminished. Indeed, MITF activity was found to be mutually exclusive to POU3F2.[27,45] The trans-state of *NRAS*^{mut} melanoma is reminiscent of senescence and correlates with overall better patient response. Indeed, once cells adapt to treatment, *P2RX7* levels go down and proliferation resumes.

Previously, accelerated growth of *P2RX7*-expressing cancers, including melanoma, has been described.[36] P2RX7 activation provokes cellular senescence and impairs tumoricidal potential of tumor-infiltrating lymphocytes (TILs) in melanoma. Induction of senescence in T effector memory cells upon P2RX7 activation is accompanied by upregulated mitochondrial ROS and cell-cycle cyclin-dependent kinase inhibitor 1A (encoding p21) levels.[46]

Figure 6. Effects of combined MEKi/CDK4/6i treatment on P2RX7 expression and function

(A and B) Effects of single and combined therapy on P2RX7 protein levels (A; 78 kDa, corresponding to the molecular weight of P2RX7A; vinculin served as a loading control [molecular weights of proteins are presented in kDa]) and P2RX7 mRNA levels (B; mean values ± SD from three biological replicates are plotted) in FACs, SACs, and prolonged (~3 months) treated SACs (protein levels only).

(C) ATP production rates after serial injection of oligomycin and rotenone/antimycin A in 0 (ctrl), 1, and 4-days-treated cells, with and without pre-injection of 100 μM BzATP (P2RX7 agonist). Both mitoATP and glycoATP production rates were assessed. Mean values ± SD from three biological replicates were calculated.

(D) Growth of MelJuso and SKMel30 cells over 14 days of combined binimetinib (MEKi) and palbociclib (CDK4/6i) inhibition with and without activation of P2RX7 (100 μM BzATP). Confluency was measured at day 14 in an IncuCyte ZOOM live-cell microscope (representative results of mean values ± SD of three technical replicates).

(E) Growth of MelJuso and SKMel30 cells in 3D over time of MEK/CDK4/6 co-inhibition.

(F) Viability of melanoma cells representing SACs (MelJuso) and FACs (SKMel30) grown in 3D for 14 days in the presence or absence of MEKi/CDK4/6i with and without BzATP measured by CellTiterGlo (mean values ± SD from three biological replicates are shown). For (B), (C), (D), and (F), statistical significance was determined by one-way ANOVA, followed by multiple comparisons test; ns, not significant; *p ≤ 0.05; ***p ≤ 0.001; ****p ≤ 0.0001.

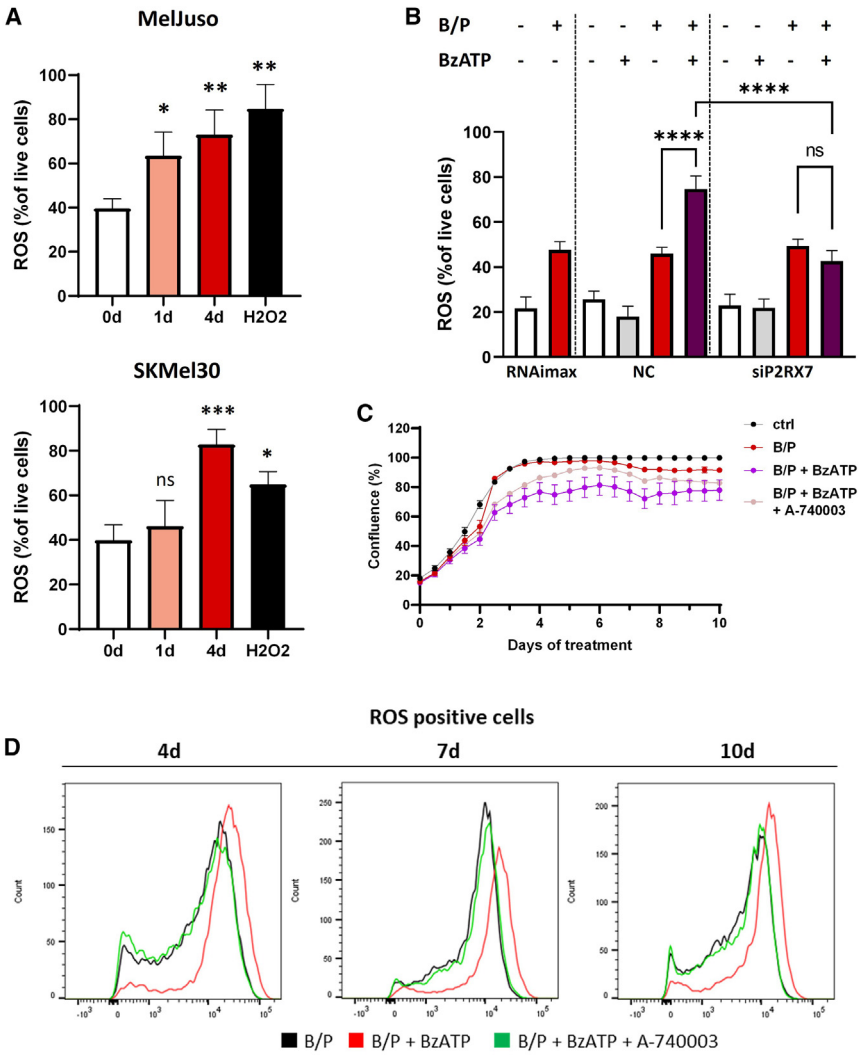

Figure 7. The impact of drug exposure on ROS production in *NRAS*^{mut} melanoma

(A) ROS production after short-term (1 and 4 days) exposure to combined MEKi/CDK4/6i therapy in MelJuso (SAC) and SKMel30 (FAC) cells. Cell exposure to H_2O_2 for 30 min served as a positive control. Mean values ± SD from three biological replicates are plotted.

(B) ROS production following P2RX7 silencing and/or activation with 100 μM BzATP in untreated or 4 days binimetinib/palbociclib-treated (B/P) MelJuso cells. RNAiMax, transfection reagent alone; NC, negative control siRNA. Bars indicate the mean values ± SD from three biological replicates.

(C) Growth curves of SACs (MelJuso) during MEK/CDK4/6 co-inhibition alone or with P2RX7 activation (100 μM BzATP) and/or P2RX7 antagonist A-740003 (1 μM), measured in an IncuCyte ZOOM live-cell microscope (representative results of mean of two technical replicates ±SEM).

(D) ROS production after 4, 7, and 10 days of MEKi (binimetinib [B]) and CDK4/6i (palbociclib [P]) treatment (B/P) with or without BzATP (100 μM) and A-740003 (1 μM). For (A) and (B), statistical significance was established by one-way ANOVA, followed by multiple comparisons test; ns, not significant; *p ≤ 0.05; **p ≤ 0.01; ***p ≤ 0.001; ****p ≤ 0.0001.

On the other hand, the progression of B16 melanoma accelerated in P2RX7-deficient mice due to a strong reduction in inflammatory infiltrates. This indicated the requirement of P2RX7 expression in tumoricidal response. Those findings are in agreement with our results demonstrating that a triple therapeutic approach involving P2RX7 activation with BzATP, CDK4/6i, and MEKi not only postpones the onset of melanoma MEKi/CDK4/6i resistance, but also impairs cellular growth in both SAC and FAC lines (Figure 6). However, administration of the P2RX7 antagonist A740003 increased immune infiltration in B16 melanoma, ultimately reducing P2RX7-dependent tumor growth (possibly due to CD4$^+$ T cell infiltration).[47] Therefore, in contrast to our findings, P2RX7 blockade has been suggested as a potent therapeutic approach and promoter of inflammatory infiltration in melanoma.[47,48] Yet, the most-used P2RX7 antagonists (A740003 and AZ10606120) have not been clinically assessed against cancer and failed in clinical trials to treat inflammatory diseases.[49] In contrast, another study using the B16 melanoma model reported that transient P2RX7 stimulation with BzATP-enhanced CD8$^+$ T cell-mediated tumor control, along with enhanced mitochondrial function and reduced expression of some exhaustion markers. Herein, P2RX7 agonism has been suggested as a novel therapeutic approach to enhance the effect of adoptive cell therapy.[50] Similarly, we found an enhanced antitumoral effect of targeted therapy in *NRAS*^{mut} melanoma cells when combined with P2RX7 activation that was abrogated by a specific P2RX7 antagonist (Figure 7C). This is in agreement with Douguet et al., who demonstrated that positive modulation of P2RX7 with HEI3090 in murine melanoma models inhibits tumor growth and enhances efficacy of anti-PD-1 immunotherapy through IL-18 production and activation of NK and CD4$^+$ T cells.[49] Thus, the selective intervention with ion signaling following activation or inhibition (depending on the cancer and the context) of P2RX7 channels might represent a promising option to delay onset of drug resistance or improve overall responses to targeted treatments.

Mechanistically, tonic P2RX7 activation supports cellular growth, while low-level and prolonged opening of this receptor results in increased cell death. Therefore, P2RX7 activity may support either tumor progression or tumoricidal responses.[51] Indeed, high levels of extracellular ATP increased Ca^{2+} influx,[52] whereas prolonged activation caused large pore opening in ATP-rich microenvironments[53] followed by augmented ROS levels and apoptosis.[33,53] Therefore, given the TCGA data and preliminary results on high P2RX7 expression in tissue samples and cell lines (Figure S14), one could speculate that excessive P2RX7 activation in *NRAS*^{mut}-treated cells might

have cytotoxic/cytostatic effects, which would not affect normal cells with lower basal P2RX7 levels. Furthermore, we showed that P2RX7 stimulation further increased already high ROS levels induced by MEKi/CDK4/6i targeted therapy. Along these lines, recent findings by Eichhoff et al. demonstrated that MEKi-treated *NRAS*^{mut} melanoma cells with elevated baseline levels of ROS are particularly sensitive to pharmacological ROS induction.[54]

Overall, we demonstrated that, by inducing augmented ROS levels, P2RX7 activation supports the cytostatic effect of combined targeted therapy and prevents the occurrence of drug resistance and, therefore, may be beneficial in the treatment of patients with melanoma harboring *NRAS* mutations. Concomitant activation of P2RX7 together with targeted treatments might be a promising approach to delay onset of drug resistance and thus prolong the window of efficacy of available or novel compounds.

Last, PI3K signaling has been previously described in *NRAS*^{mut} melanoma drug resistance.[2] During early drug exposure in cells of the trans-state, we confirmed the downregulation of downstream PI3K targets. This is in line with previous findings where high levels of eATP and activation of P2RX7 were found to block the PI3K pathway, ultimately resulting in cellular growth inhibition, while physiological Ca^{2+} levels were required to maintain basal PI3K signaling.[55]

To our knowledge, P2RX7 has not been previously implicated in *NRAS*^{mut} melanoma drug responses. Here we show that P2RX7 is transiently induced in melanoma cells responding to MEKi/CDK4/6i, but expression returns to baseline once cells have adapted to treatment, as evidenced by their re-entering the cell cycle and resuming proliferation. Concomitant induction of P2RX7 together with joint inhibition of MAPK signaling and cell-cycle progression could therefore represent a promising combination to prolong treatment effects and delay onset of targeted drug resistance. Moreover, P2RX7 expression levels could be explored in larger cohorts of patients with melanoma for their potential as a marker indicating the stage of response to targeted treatments.

Limitations of the study

The experimental approach to sequence *NRAS*^{mut} melanoma cell lines with Drop-Seq turned out to yield high-quality scRNA-seq data suitable for the tracing of distinct cellular states emerging at different time points under targeted inhibitor treatment. However, we are aware that 10× Genomics Chromium (10×) can provide higher sensitivity (capturing more transcripts), which could be used to confirm the states we describe here and/or to potentially refine some of the transcriptional profiles or to find additional ones that we might have missed.

The very strong effect of MEK and CDK4/6 co-inhibition in our 3D models masked potential effects of P2RX7 activation. Once more potent activators of P2RX7 are available, such compounds should be tested alongside other targeted drug combinations in *NRAS*^{mut} mouse models to show the effects of P2RX7 activation. Also, the P2RX7-positive modulator HEI3090 could be tested together with MEKi/CDK4/6 co-inhibition in an *NRAS*^{mut} melanoma in mouse model. Finally, to extend our findings on the induction of ROS, other scavengers could be applied. We have tested NAC (N-acetyl-L-cysteine) and did not see an efficient scavenging effect for ROS, but with other scavengers or different experimental setups, this could possibly be achieved.

STAR★METHODS

Detailed methods are provided in the online version of this paper and include the following:

- KEY RESOURCES TABLE
- RESOURCE AVAILABILITY
  - Lead contact
  - Materials availability
  - Data and code availability
- EXPERIMENTAL MODEL AND STUDY PARTICIPANT DETAILS
  - Cell lines
  - 3D melanoma model
- METHOD DETAILS
  - Reagents
  - Cell viability assays
  - Immunoblotting and antibodies
  - Immunofluorescence staining
  - Caspase-3 activity assay
  - Senescence beta-galactosidase (SA-βgal) activity assay
  - Real-time proliferation assay
  - Single-cell RNA-sequencing
  - Single-cell RNA-sequencing data analysis
  - RNA extraction and quantitative PCR
  - Small interfering RNAs and transfection
  - Flow cytometry and ROS activity
  - Seahorse and real-time ATP rate assay
  - ATP consumption and production assay
  - Survival analysis
  - Human melanoma samples and P2RX7 immunohistochemistry
- QUANTIFICATION AND STATISTICAL ANALYSIS

SUPPLEMENTAL INFORMATION

Supplemental information can be found online at https://doi.org/10.1016/j.celrep.2023.112696.

ACKNOWLEDGMENTS

We thank Prof. Dagmar Kulms (University Clinics Dresden) for sharing M20 cells with us and Dr. Elisabeth Letellier for critically reading the manuscript. We thank Vincent Gureghian for identifying senescence in MelJuso and for valuable discussions on cellular responses to drugs, Dr. Mirjana Efremova and Dr. Anthoula Gaigneaux for valuable advice on single-cell data analysis, and Dr. Vitaly Pozdeev for expert support on FACS analysis. The work by T.R. and S.M. is supported by the Luxembourg National Research Fond (FNR) PRIDE DTU CriTiCS (grant reference 10907093). M.M. is supported by an FNR PEARL P16/BM/11192868 grant. P.V.N. was supported by the Luxembourg FNR CORE grant C21/BM/15739125/DIOMEDES.

AUTHOR CONTRIBUTIONS

T.R. and S.K. designed the study. T.R. and K.G. performed the scRNA-seq experiments, with supervision from A.S. T.R. analyzed and interpreted the scRNA-seq data, supervised by S.M. and P.V.N. T.R. and P.V.N. analyzed and interpreted the TCGA data. Experimental validations were done by T.R., D.P., and C.M. supported by J.R.P. and J.P.W. M.M. and K.B.M.F. analyzed and interpreted histological and immunohistochemical data. S.K. and A.S. acquired funding. S.K. and S.M. supervised the project. T.R., S.M., and S.K. wrote the initial draft of the manuscript. All authors read and edited the final draft of the manuscript.

DECLARATION OF INTERESTS

The authors declare no competing interests.

Received: November 30, 2022
Revised: May 1, 2023
Accepted: June 9, 2023
Published: June 29, 2023

REFERENCES

1. Hodis, E., Watson, I.R., Kryukov, G.V., Arold, S.T., Imielinski, M., Theurillat, J.-P., Nickerson, E., Auclair, D., Li, L., Place, C., et al. (2012). A landscape of driver mutations in melanoma. Cell *150*, 251–263. https://doi.org/10.1016/j.cell.2012.06.024.
2. Randic, T., Kozar, I., Margue, C., Utikal, J., and Kreis, S. (2021). NRAS mutant melanoma: Towards better therapies. Cancer Treat Rev. *99*, 102238. https://doi.org/10.1016/j.ctrv.2021.102238.
3. Switzer, B., Puzanov, I., Skitzki, J.J., Hamad, L., and Ernstoff, M.S. (2022). Managing Metastatic Melanoma in 2022: A Clinical Review. JCO Oncol. Pract. *18*, 335–351. https://doi.org/10.1200/OP.21.00686.
4. Salzmann, M., Pawlowski, J., Loquai, C., Rafei-Shamsabadi, D.A., Meiss, F., Ugurel, S., Schadendorf, D., Meier, F., Enk, A.H., and Hassel, J.C. (2022). MEK inhibitors for pre-treated, NRAS-mutated metastatic melanoma: A multi-centre, retrospective study. Eur. J. Cancer *166*, 24–32. https://doi.org/10.1016/j.ejca.2022.02.008.
5. Garutti, M., Targato, G., Buriolla, S., Palmero, L., Minisini, A.M., and Puglisi, F. (2021). CDK4/6 Inhibitors in Melanoma: A Comprehensive Review. Cells *10*, 1334. https://doi.org/10.3390/cells10061334.
6. Ascierto, P.A., Schadendorf, D., Berking, C., Agarwala, S.S., van Herpen, C.M., Queirolo, P., Blank, C.U., Hauschild, A., Beck, J.T., St-Pierre, A., et al. (2013). MEK162 for patients with advanced melanoma harbouring NRAS or Val600 BRAF mutations: a non-randomised, open-label phase 2 study. Lancet Oncol. *14*, 249–256. https://doi.org/10.1016/S1470-2045(13)70024-X.
7. Dummer, R., Schadendorf, D., Ascierto, P.A., Arance, A., Dutriaux, C., Di Giacomo, A.M., Rutkowski, P., Del Vecchio, M., Gutzmer, R., Mandala, M., et al. (2017). Binimetinib versus dacarbazine in patients with advanced NRAS-mutant melanoma (NEMO): a multicentre, open-label, randomised, phase 3 trial. Lancet Oncol. *18*, 435–445. https://doi.org/10.1016/S1470-2045(17)30180-8.
8. Michielin, O., van Akkooi, A.C.J., Ascierto, P.A., Dummer, R., and Keilholz, U.; ESMO Guidelines Committee. (2019). Cutaneous melanoma: ESMO Clinical Practice Guidelines for diagnosis, treatment and follow-up†. Ann. Oncol. *30*, 1884–1901. https://doi.org/10.1093/annonc/mdz411.
9. Lau, P.K.H., Ascierto, P.A., and McArthur, G. (2016). Melanoma: the intersection of molecular targeted therapy and immune checkpoint inhibition. Curr. Opin. Immunol. *39*, 30–38. https://doi.org/10.1016/j.coi.2015.12.006.
10. Van Herpen, C., Postow, M.A., Carlino, M.S., Kalkavan, H., Weise, A., Amaria, R.N., Vos, F.D., Carvajal, R.D., Matano, A., Bhansali, S., et al. (2015). 3300 A phase 1b/2 study of ribociclib (LEE011; CDK4/6 inhibitor) in combination with binimetinib (MEK162; MEK inhibitor) in patients with NRAS-mutant melanoma. Eur. J. Cancer *51*, S663.
11. Teh, J.L.F., Cheng, P.F., Purwin, T.J., Nikbakht, N., Patel, P., Chervoneva, I., Ertel, A., Fortina, P.M., Kleiber, I., HooKim, K., et al. (2018). In Vivo E2F Reporting Reveals Efficacious Schedules of MEK1/2-CDK4/6 Targeting and mTOR-S6 Resistance Mechanisms. Cancer Discov. *8*, 568–581. https://doi.org/10.1158/2159-8290.CD-17-0699.
12. Schuler, M.H., Ascierto, P.A., De Vos, F.Y.F.L., Postow, M.A., Van Herpen, C.M., Carlino, M.S., Sosman, J.A., Berking, C., Long, G.V., and Weise, A. (2017). Phase 1b/2 trial of ribociclib+ binimetinib in metastatic NRAS-mutant melanoma: Safety, efficacy, and recommended phase 2 dose (RP2D). J. Clin. Oncol. *35*, 9519.
13. Hayes, T.K., Luo, F., Cohen, O., Goodale, A.B., Lee, Y., Pantel, S., Bagul, M., Piccioni, F., Root, D.E., Garraway, L.A., et al. (2019). A Functional Landscape of Resistance to MEK1/2 and CDK4/6 Inhibition in NRAS-Mutant Melanoma. Cancer Res. *79*, 2352–2366. https://doi.org/10.1158/0008-5472.CAN-18-2711.
14. Romano, G., Chen, P.-L., Song, P., McQuade, J.L., Liang, R.J., Liu, M., Roh, W., Duose, D.Y., Carapeto, F.C.L., Li, J., et al. (2018). A Preexisting Rare PIK3CA(E545K) Subpopulation Confers Clinical Resistance to MEK plus CDK4/6 Inhibition in NRAS Melanoma and Is Dependent on S6K1 Signaling. Cancer Discov. *8*, 556–567. https://doi.org/10.1158/2159-8290.CD-17-0745.
15. Rambow, F., Rogiers, A., Marin-Bejar, O., Aibar, S., Femel, J., Dewaele, M., Karras, P., Brown, D., Chang, Y.H., Debiec-Rychter, M., et al. (2018). Toward Minimal Residual Disease-Directed Therapy in Melanoma. Cell *174*, 843–855.e19. https://doi.org/10.1016/j.cell.2018.06.025.
16. Baron, M., Tagore, M., Hunter, M.V., Kim, I.S., Moncada, R., Yan, Y., Campbell, N.R., White, R.M., and Yanai, I. (2020). The Stress-Like Cancer Cell State Is a Consistent Component of Tumorigenesis. Cell Syst. *11*, 536–546.e7. https://doi.org/10.1016/j.cels.2020.08.018.
17. Marin-Bejar, O., Rogiers, A., Dewaele, M., Femel, J., Karras, P., Pozniak, J., Bervoets, G., Van Raemdonck, N., Pedri, D., Swings, T., et al. (2021). Evolutionary predictability of genetic versus nongenetic resistance to anticancer drugs in melanoma. Cancer Cell *39*, 1135–1149.e8. https://doi.org/10.1016/j.ccell.2021.05.015.
18. Binder, H., Schmidt, M., Loeffler-Wirth, H., Mortensen, L.S., and Kunz, M. (2021). Melanoma Single-Cell Biology in Experimental and Clinical Settings. J. Clin. Med. *10*, 506. https://doi.org/10.3390/jcm10030506.
19. Wouters, J., Kalender-Atak, Z., Minnoye, L., Spanier, K.I., De Waegeneer, M., Bravo González-Blas, C., Mauduit, D., Davie, K., Hulselmans, G., Najem, A., et al. (2020). Robust gene expression programs underlie recurrent cell states and phenotype switching in melanoma. Nat. Cell Biol. *22*, 986–998. https://doi.org/10.1038/s41556-020-0547-3.
20. Janho Dit Hreich, S., Benzaquen, J., Hofman, P., and Vouret-Craviari, V. (2021). To inhibit or to boost the ATP/P2RX7 pathway to fight cancer-that is the question. Purinergic Signal. *17*, 619–631. https://doi.org/10.1007/s11302-021-09811-9.
21. Street, K., Risso, D., Fletcher, R.B., Das, D., Ngai, J., Yosef, N., Purdom, E., and Dudoit, S. (2018). Slingshot: cell lineage and pseudotime inference for single-cell transcriptomics. BMC Genom. *19*, 477.
22. Tirosh, I., Izar, B., Prakadan, S.M., Wadsworth, M.H., 2nd, Treacy, D., Trombetta, J.J., Rotem, A., Rodman, C., Lian, C., Murphy, G., et al. (2016). Dissecting the multicellular ecosystem of metastatic melanoma by single-cell RNA-seq. Science *352*, 189–196. https://doi.org/10.1126/science.aad0501.
23. Titz, B., Lomova, A., Le, A., Hugo, W., Kong, X., Ten Hoeve, J., Friedman, M., Shi, H., Moriceau, G., Song, C., et al. (2016). JUN dependency in distinct early and late BRAF inhibition adaptation states of melanoma. Cell Discov. *2*, 16028. https://doi.org/10.1038/celldisc.2016.28.
24. Qiu, X., Mao, Q., Tang, Y., Wang, L., Chawla, R., Pliner, H.A., and Trapnell, C. (2017). Reversed graph embedding resolves complex single-cell trajectories. Nat. Methods *14*, 979–982. https://doi.org/10.1038/nmeth.4402.

25. Karras, P., Bordeu, I., Pozniak, J., Nowosad, A., Pazzi, C., Van Raemdonck, N., Landeloos, E., Van Herck, Y., Pedri, D., Bervoets, G., et al. (2022). A cellular hierarchy in melanoma uncouples growth and metastasis. Nature *610*, 190–198. https://doi.org/10.1038/s41586-022-05242-7.

26. Liberzon, A., Birger, C., Thorvaldsdóttir, H., Ghandi, M., Mesirov, J.P., and Tamayo, P. (2015). The Molecular Signatures Database (MSigDB) hallmark gene set collection. Cell Syst. *1*, 417–425. https://doi.org/10.1016/j.cels.2015.12.004.

27. Rambow, F., Marine, J.-C., and Goding, C.R. (2019). Melanoma plasticity and phenotypic diversity: therapeutic barriers and opportunities. Genes Dev. *33*, 1295–1318. https://doi.org/10.1101/gad.329771.119.

28. Xia, Y., Zhou, Y., Han, H., Li, P., Wei, W., and Lin, N. (2019). lncRNA NEAT1 facilitates melanoma cell proliferation, migration, and invasion via regulating miR-495-3p and E2F3. J. Cell. Physiol. *234*, 19592–19601. https://doi.org/10.1002/jcp.28559.

29. Li, F., Li, X., Qiao, L., Liu, W., Xu, C., and Wang, X. (2019). MALAT1 regulates miR-34a expression in melanoma cells. Cell Death Dis. *10*, 389. https://doi.org/10.1038/s41419-019-1620-3.

30. Luan, W., Li, L., Shi, Y., Bu, X., Xia, Y., Wang, J., Djangmah, H.S., Liu, X., You, Y., and Xu, B. (2016). Long non-coding RNA MALAT1 acts as a competing endogenous RNA to promote malignant melanoma growth and metastasis by sponging miR-22. Oncotarget *7*, 63901–63912. https://doi.org/10.18632/oncotarget.11564.

31. Aibar, S., González-Blas, C.B., Moerman, T., Huynh-Thu, V.A., Imrichova, H., Hulselmans, G., Rambow, F., Marine, J.-C., Geurts, P., Aerts, J., et al. (2017). SCENIC: single-cell regulatory network inference and clustering. Nat. Methods *14*, 1083–1086. https://doi.org/10.1038/nmeth.4463.

32. Tiwari, N., Tiwari, V.K., Waldmeier, L., Balwierz, P.J., Arnold, P., Pachkov, M., Meyer-Schaller, N., Schübeler, D., van Nimwegen, E., and Christofori, G. (2013). Sox4 is a master regulator of epithelial-mesenchymal transition by controlling Ezh2 expression and epigenetic reprogramming. Cancer Cell *23*, 768–783. https://doi.org/10.1016/j.ccr.2013.04.020.

33. Savio, L.E.B., de Andrade Mello, P., da Silva, C.G., and Coutinho-Silva, R. (2018). The P2X7 Receptor in Inflammatory Diseases: Angel or Demon? Front. Pharmacol. *9*, 52. https://doi.org/10.3389/fphar.2018.00052.

34. Surprenant, A., Rassendren, F., Kawashima, E., North, R.A., and Buell, G. (1996). The cytolytic P2Z receptor for extracellular ATP identified as a P2X receptor (P2X7). Science *272*, 735–738. https://doi.org/10.1126/science.272.5262.735.

35. Rabelo, I.L.A., Arnaud-Sampaio, V.F., Adinolfi, E., Ulrich, H., and Lameu, C. (2021). Cancer Metabostemness and Metabolic Reprogramming via P2X7 Receptor. Cells *10*, 1782. https://doi.org/10.3390/cells10071782.

36. Lara, R., Adinolfi, E., Harwood, C.A., Philpott, M., Barden, J.A., Di Virgilio, F., and McNulty, S. (2020). P2X7 in Cancer: From Molecular Mechanisms to Therapeutics. Front. Pharmacol. *11*, 793. https://doi.org/10.3389/fphar.2020.00793.

37. Moore, S.F., and MacKenzie, A.B. (2009). NADPH oxidase NOX2 mediates rapid cellular oxidation following ATP stimulation of endotoxin-primed macrophages. J. Immunol. *183*, 3302–3308. https://doi.org/10.4049/jimmunol.0900394.

38. Wang, B., and Sluyter, R. (2013). P2X7 receptor activation induces reactive oxygen species formation in erythroid cells. Purinergic Signal. *9*, 101–112. https://doi.org/10.1007/s11302-012-9335-2.

39. Pasha, N., and Turner, N.C. (2021). Understanding and overcoming tumor heterogeneity in metastatic breast cancer treatment. Nat. cancer *2*, 680–692. https://doi.org/10.1038/s43018-021-00229-1.

40. Christensen, D.S., Ahrenfeldt, J., Sokač, M., Kisistók, J., Thomsen, M.K., Maretty, L., McGranahan, N., and Birkbak, N.J. (2022). Treatment Represents a Key Driver of Metastatic Cancer Evolution. Cancer Res. *82*, 2918–2927. https://doi.org/10.1158/0008-5472.CAN-22-0562.

41. Su, Y., Bintz, M., Yang, Y., Robert, L., Ng, A.H.C., Liu, V., Ribas, A., Heath, J.R., and Wei, W. (2019). Phenotypic heterogeneity and evolution of melanoma cells associated with targeted therapy resistance. PLoS Comput. Biol. *15*, e1007034. https://doi.org/10.1371/journal.pcbi.1007034.

42. Dagogo-Jack, I., and Shaw, A.T. (2018). Tumour heterogeneity and resistance to cancer therapies. Nat. Rev. Clin. Oncol. *15*, 81–94. https://doi.org/10.1038/nrclinonc.2017.166.

43. Su, Y., Ko, M.E., Cheng, H., Zhu, R., Xue, M., Wang, J., Lee, J.W., Frankiw, L., Xu, A., Wong, S., et al. (2020). Multi-omic single-cell snapshots reveal multiple independent trajectories to drug tolerance in a melanoma cell line. Nat. Commun. *11*, 2345. https://doi.org/10.1038/s41467-020-15956-9.

44. Chiappinelli, K.B., Strissel, P.L., Desrichard, A., Li, H., Henke, C., Akman, B., Hein, A., Rote, N.S., Cope, L.M., Snyder, A., et al. (2015). Inhibiting DNA Methylation Causes an Interferon Response in Cancer via dsRNA Including Endogenous Retroviruses. Cell *162*, 974–986. https://doi.org/10.1016/j.cell.2015.07.011.

45. Goodall, J., Carreira, S., Denat, L., Kobi, D., Davidson, I., Nuciforo, P., Sturm, R.A., Larue, L., and Goding, C.R. (2008). Brn-2 represses microphthalmia-associated transcription factor expression and marks a distinct subpopulation of microphthalmia-associated transcription factor-negative melanoma cells. Cancer Res. *68*, 7788–7794. https://doi.org/10.1158/0008-5472.CAN-08-1053.

46. Romagnani, A., Rottoli, E., Mazza, E.M.C., Rezzonico-Jost, T., De Ponte Conti, B., Proietti, M., Perotti, M., Civanelli, E., Perruzza, L., Catapano, A.L., et al. (2020). P2X7 Receptor Activity Limits Accumulation of T Cells within Tumors. Cancer Res. *80*, 3906–3919. https://doi.org/10.1158/0008-5472.CAN-19-3807.

47. De Marchi, E., Orioli, E., Pegoraro, A., Sangaletti, S., Portararo, P., Curti, A., Colombo, M.P., Di Virgilio, F., and Adinolfi, E. (2019). The P2X7 receptor modulates immune cells infiltration, ectonucleotidases expression and extracellular ATP levels in the tumor microenvironment. Oncogene *38*, 3636–3650. https://doi.org/10.1038/s41388-019-0684-y.

48. Pegoraro, A., De Marchi, E., Ferracin, M., Orioli, E., Zanoni, M., Bassi, C., Tesei, A., Capece, M., Dika, E., Negrini, M., et al. (2021). P2X7 promotes metastatic spreading and triggers release of miRNA-containing exosomes and microvesicles from melanoma cells. Cell Death Dis. *12*, 1088. https://doi.org/10.1038/s41419-021-04378-0.

49. Douguet, L., Janho Dit Hreich, S., Benzaquen, J., Seguin, L., Juhel, T., Dezitter, X., Duranton, C., Ryffel, B., Kanellopoulos, J., Delarasse, C., et al. (2021). A small-molecule P2RX7 activator promotes anti-tumor immune responses and sensitizes lung tumor to immunotherapy. Nat. Commun. *12*, 653. https://doi.org/10.1038/s41467-021-20912-2.

50. Wanhainen, K.M., Peng, C., Zhou, M.H., Macedo, B.d.G., O'Flanagan, S., Yang, T., Kelekar, A., Burbach, B.J., Borges da Silva, H., and Jameson, S.C. (2022). P2RX7 Enhances Tumor Control by CD8+ T Cells in Adoptive Cell Therapy. Cancer Immunol. Res. *10*, 871–884. https://doi.org/10.1158/2326-6066.CIR-21-0691.

51. Zanoni, M., Sarti, A.C., Zamagni, A., Cortesi, M., Pignatta, S., Arienti, C., Tebaldi, M., Sarnelli, A., Romeo, A., Bartolini, D., et al. (2022). Irradiation causes senescence, ATP release, and P2X7 receptor isoform switch in glioblastoma. Cell Death Dis. *13*, 80. https://doi.org/10.1038/s41419-022-04526-0.

52. Di Virgilio, F., Dal Ben, D., Sarti, A.C., Giuliani, A.L., and Falzoni, S. (2017). The P2X7 Receptor in Infection and Inflammation. Immunity *47*, 15–31. https://doi.org/10.1016/j.immuni.2017.06.020.

53. Benzaquen, J., Dit Hreich, S.J., Heeke, S., Juhel, T., Lalvee, S., Bauwens, S., Saccani, S., Lenormand, P., Hofman, V., Butori, M., et al. (2020). P2RX7B is a new theranostic marker for lung adenocarcinoma patients. Theranostics *10*, 10849–10860. https://doi.org/10.7150/thno.48229.

54. Eichhoff, O.M., Stoffel, C.I., Käsler, J., Briker, L., Turko, P., Karsai, G., Zila, N., Paulitschke, V., Cheng, P.F., Leitner, A., et al. (2023). ROS Induction Targets Persister Cancer Cells with Low Metabolic Activity in NRAS-Mutated Melanoma. Cancer Res. *83*, 1128–1146. https://doi.org/10.1158/0008-5472.CAN-22-1826.

55. Bian, S., Sun, X., Bai, A., Zhang, C., Li, L., Enjyoji, K., Junger, W.G., Robson, S.C., and Wu, Y. (2013). P2X7 integrates PI3K/AKT and

AMPK-PRAS40-mTOR signaling pathways to mediate tumor cell death. PLoS One *8*, e60184. https://doi.org/10.1371/journal.pone.0060184.

56. Stuart, T., Butler, A., Hoffman, P., Hafemeister, C., Papalexi, E., Mauck, W.M., 3rd, Hao, Y., Stoeckius, M., Smibert, P., and Satija, R. (2019). Comprehensive Integration of Single-Cell Data. Cell *177*, 1888–1902.e21. https://doi.org/10.1016/j.cell.2019.05.031.
57. Subramanian, A., Tamayo, P., Mootha, V.K., Mukherjee, S., Ebert, B.L., Gillette, M.A., Paulovich, A., Pomeroy, S.L., Golub, T.R., Lander, E.S., and Mesirov, J.P. (2005). Gene set enrichment analysis: a knowledge-based approach for interpreting genome-wide expression profiles. Proc. Natl. Acad. Sci. USA *102*, 15545–15550. https://doi.org/10.1073/pnas.0506580102.
58. Korotkevich, G., Sukhov, V., Budin, N., Shpak, B., Artyomov, M.N., and Sergushichev, A. (2016). Fast gene set enrichment analysis. Preprint at bioRxiv. https://doi.org/10.1101/060012.
59. Ianevski, A., He, L., Aittokallio, T., and Tang, J. (2017). SynergyFinder: a web application for analyzing drug combination dose-response matrix data. Bioinformatics *33*, 2413–2415. https://doi.org/10.1093/bioinformatics/btx162.
60. Haan, C., and Behrmann, I. (2007). A cost effective non-commercial ECL-solution for Western blot detections yielding strong signals and low background. J. Immunol. Methods *318*, 11–19. https://doi.org/10.1016/j.jim.2006.07.027.
61. Cesi, G., Walbrecq, G., Zimmer, A., Kreis, S., and Haan, C. (2017). ROS production induced by BRAF inhibitor treatment rewires metabolic processes affecting cell growth of melanoma cells. Mol. Cancer *16*, 102. https://doi.org/10.1186/s12943-017-0667-y.
62. Macosko, E.Z., Basu, A., Satija, R., Nemesh, J., Shekhar, K., Goldman, M., Tirosh, I., Bialas, A.R., Kamitaki, N., Martersteck, E.M., et al. (2015). Highly Parallel Genome-wide Expression Profiling of Individual Cells Using Nanoliter Droplets. Cell *161*, 1202–1214. https://doi.org/10.1016/j.cell.2015.05.002.
63. Walter, J., Bolognin, S., Antony, P.M.A., Nickels, S.L., Poovathingal, S.K., Salamanca, L., Magni, S., Perfeito, R., Hoel, F., Qing, X., et al. (2019). Neural Stem Cells of Parkinson's Disease Patients Exhibit Aberrant Mitochondrial Morphology and Functionality. Stem Cell Rep. *12*, 878–889. https://doi.org/10.1016/j.stemcr.2019.03.004.
64. Hao, Y., Hao, S., Andersen-Nissen, E., Mauck, W.M., 3rd, Zheng, S., Butler, A., Lee, M.J., Wilk, A.J., Darby, C., Zager, M., et al. (2021). Integrated analysis of multimodal single-cell data. Cell *184*, 3573–3587.e29. https://doi.org/10.1016/j.cell.2021.04.048.
65. Mootha, V.K., Lindgren, C.M., Eriksson, K.-F., Subramanian, A., Sihag, S., Lehar, J., Puigserver, P., Carlsson, E., Ridderstråle, M., Laurila, E., et al. (2003). PGC-1alpha-responsive genes involved in oxidative phosphorylation are coordinately downregulated in human diabetes. Nat. Genet. *34*, 267–273. https://doi.org/10.1038/ng1180.
66. Suo, S., Zhu, Q., Saadatpour, A., Fei, L., Guo, G., and Yuan, G.-C. (2018). Revealing the Critical Regulators of Cell Identity in the Mouse Cell Atlas. Cell Rep. *25*, 1436–1445.e3. https://doi.org/10.1016/j.celrep.2018.10.045.
67. Kozar, I., Philippidou, D., Margue, C., Gay, L.A., Renne, R., and Kreis, S. (2021). Cross-Linking Ligation and Sequencing of Hybrids (qCLASH) Reveals an Unpredicted miRNA Targetome in Melanoma Cells. Cancers *13*, 1096. https://doi.org/10.3390/cancers13051096.

STAR★METHODS

KEY RESOURCES TABLE

REAGENT or RESOURCE	SOURCE	IDENTIFIER
Antibodies		
Rabbit monoclonal anti-phospho-RB	Cell Signaling Technology	Cat# 8180; RRID: AB_10950972
Mouse monoclonal anti-RB	Cell Signaling Technology	Cat# 9309; RRID: AB_823629
Rabbit polyclonal anti-phospho-ERK1/2	Cell Signaling Technology	Cat# 9101; RRID: AB_331646
Mouse polyclonal anti-ERK1/2	Cell Signaling Technology	Cat# 9102; RRID: AB_330744
Rabbit monoclonal anti-phospho-S6 ribosomal protein	Cell Signaling Technology	Cat# 2211; RRID: AB_331679
Rabbit monoclonal anti-S6 ribosomal protein	Cell Signaling Technology	Cat# 2217; RRID: AB_331355
Rabbit monoclonal anti-phospho-MEK1/2	Cell Signaling Technology	Cat# 9154; RRID: AB_2138017
Mouse monoclonal anti-MEK1/2	Cell Signaling Technology	Cat# 4694; RRID: AB_10695868
Rabbit monoclonal anti-Vinculin	Cell Signaling Technology	Cat# 13901; RRID: AB_2728768
Rabbit monoclonal anti-P2RX7	Cell Signaling Technology	Cat# 13809; RRID: AB_2798319
Rabbit polyclonal anti-P2RX7	Sigma Aldrich	Cat# HPA034968; RRID: AB_10673105
Anti-mouse IgG, HRP-linked Antibody	Cell Signaling Technology	Cat# 7076; RRID: AB_330924
Anti-rabbit IgG, HRP-linked Antibody	Cell Signaling Technology	Cat# 7074; RRID: AB_2099233
Rabbit monoclonal anti-Ki-67	Abcam	Cat# ab16667; RRID: AB_302459
Donkey anti-Rabbit IgG (H+L) Highly Cross-Adsorbed Secondary Antibody, Alexa Fluor 647	Thermo Fisher Scientific, Invitrogen	Cat# A-31573; RRID: AB_2536183
Chemicals, peptides, and recombinant proteins		
Binimetinib (MEK-162)	MedKoo Biosciences	Cat# 205531
Cobimetinib (GDC-0973, RG7420)	MedChemExpress	Cat# HY-13064
Trametinib (GSK1120212)	Selleck Chemicals	Cat# S2673
Palbociclib (PD-0332991)	Selleck Chemicals	Cat# S1116
Ribociclib (LEE011)	Chemietek	Cat# CT-LEE011
Staurosporine	Cayman chemicals	Cat# 81590-10
KN-62	Selleck Chemicals	Cat# S7422
A-740003	Selleck Chemicals	Cat# S0826
BzATP triethylammonium salt	Santa Cruz Biotechnology	Cat# sc-203862
Phosphate buffer saline (PBS)	Thermo Fisher Scientific, Gibco	Cat# 18912014
RPMI 1640 Medium, GlutaMAX™ Supplement	Thermo Fisher Scientific, Gibco	Cat# 61870010
Fetal bovine serum	Thermo Fisher Scientific, Gibco	Cat# 11573397
Penicillin-Streptomycin (10,000 U/mL)	Thermo Fisher Scientific, Gibco	Cat# 15140122
HBSS, calcium, magnesium, no phenol red	Thermo Fisher Scientific, Gibco	Cat# 14025092
DAPI	Thermo Fisher Scientific, Invitrogen	Cat# D1306
Triton X-100	Merck Life Sciences BV	Cat# T8787-100ML
Ac-DEVD-AFC	Santa Cruz Biotechnology	Cat# sc-311274
Barcoded beads	ChemGenes Corp	Cat# Macosko-2011-10
Sarkosyl	Teknova	Cat# S3376
Ficoll	Sigma Aldrich	Cat# F5415
EDTA	Thermo Fisher Scientific, Fisher Scientific	Cat# BP2482-500
Tris-HCl	Thermo Fisher Scientific, Fisher Scientific	Cat# BP1757-500

(*Continued on next page*)

Continued

REAGENT or RESOURCE	SOURCE	IDENTIFIER
DTT	Teknova	Cat# D9750
Droplet generator oil	BIO-RAD	Cat# 1864006
Perfluorooctanol	Synquest	Cat# 2101-3-20
RT SSC buffer	Teknova	Cat# S0282
Reverse Transcriptase mix	Thermo Fisher Scientific, Thermo Scientific	Cat# EP0751
Lipofectamine RNAiMAX	Thermo Fisher Scientific, Invitrogen	Cat# 13778150
iTaq Universal SYBR Green Supermix, 5.000X20ul reactions	BIO-RAD	Cat# 1725125
CM-H2DCFDA	Thermo Fisher Scientific, Invitrogen	Cat# C6827
Hydrogen peroxide 30%	Carl ROTH	Cat# 8070.2
Live/Dead Fixable Near-IR Dead Cell stain	Thermo Fisher Scientific, Invitrogen	Cat# L34976
Seahorse XF RPMI medium, pH 7.4	Agilent Technologies	Cat# 103576-100
Oligomycin A	Bio-techne	Cat# 4110
Rotenone	Sigma Aldrich	Cat# R8875
Antimycin A	Sigma Aldrich	Cat# A8674
Hoechst 33342	Thermo Fisher Scientific, Thermo Scientific	Cat# 62249
Critical commercial assays		
Senescence β-Galactosidase Staining Kit	Cell Signaling Technology	Cat# 9860
Quick-RNA MiniPrep Kit (200 Preps)	ZYMO Research	Cat# R1055
iScriptTM cDNA Synthesis kit	BIO-RAD	Cat# ZR1055
ATP Determination Kit	Thermo Fisher Scientific, Invitrogen	Cat# A22066
CellTiterGLO 3D Viability assay	Promega	Cat# G9683
Deposited data		
Single-cell RNA Seq FASTQ files	This paper	GEO: GSE230538
Gene expression matrix	Rambow et al.[15]	GEO: GSE116237
Experimental models: Cell lines		
SKMel30	DSMZ Leibniz Institut	Cat# ACC-151
MelJuso	DSMZ Leibniz Institut	Cat# ACC-74
IPC298	DSMZ Leibniz Institut	Cat# ACC-251
M20	Dr. Dagmar Kulms	N/A
Oligonucleotides		
P2RX7 primer	Eurogentec	(forward):CGGAAAGAGCCTGTCATCA (reverse):TGTAGTCTGCGGTGTCAAAGA
HPRT primer	Eurogentec	(forward):TGGACAGGACTGAACGTCTT (reverse):GAGCACACAGAGGGCTACAA
TBP primer	Eurogentec	(forward):TGATCTTTGCAGTGACCCAG (reverse):CGCTGGAACTCGTCTCACTA
PPIA primer	Eurogentec	(forward):CAGACAAGGTCCCAAAGACA (reverse):CCATTATGGCGTGTGAAGTC
Software and algorithms		
Seurat, v4.0.2	Stuart et al.[56]	https://satijalab.org/seurat/
Monocle 2	Trapnell et al.[24]	http://cole-trapnell-lab.github.io/monocle-release/

(*Continued on next page*)

Continued

REAGENT or RESOURCE	SOURCE	IDENTIFIER
GSEA, v4.0.3	Subramanian et al.[57]	https://www.gsea-msigdb.org/gsea/index.jsp
fGSEA v1.21	Korotkevich et al.[58]	http://bioconductor.org/packages/devel/bioc/vignettes/fgsea/inst/doc/fgsea-tutorial.html
SCENIC v1.2.0	Aibar et al.[31]	https://scenic.aertslab.org/
Slingshot	Street et al.[21]	Bioconductor
CFX Manager software	BIO-RAD	Cat# 1845000
FlowJo software, v10.8.1	Treestar Inc	https://www.flowjo.com/
Prism, v9	GraphPad Software	https://www.graphpad.com/scientific-software/prism/
Other		
Cytation 5 Cell Imaging Multi-Mode Reader	BioTek	N/A
IncuCyte ZOOM live cell microscope	Essen BioScience	N/A
NanoDrop2000 Spectrophotometer	Isogen Life Science	N/A
Seahorse Xfe96 analyser	Agilent Technologies	N/A

RESOURCE AVAILABILITY

Lead contact

Further requests for resources and reagents should be directed to the lead contact.

Materials availability

This study did not generate new unique reagents.

Data and code availability

- The scRNA-seq data has been deposited in GEO under the accession number GSE230538.
- The code employed for the scRNA-seq data analysis is publicaly available on GitHub at the public repository: https://github.com/tijanaran/NRAS-mutant_melanoma_Single-cell_RNA_Seq.
- Any additional information required to reanalyze the data reported in this paper is available from the lead contact upon request.

EXPERIMENTAL MODEL AND STUDY PARTICIPANT DETAILS

Cell lines

The *NRAS*^{mut} melanoma cell lines used in this study SKMel30, IPC298, and MelJuso were purchased from DSMZ (Leibniz Institute), and M20 was provided by Dr. D. Kulms (University of Dresden, Germany). The MEKi/CDK4/6i-resistant melanoma cell lines were generated by exposure of drug-sensitive cell lines to 1 μM Palbociclib and 1xIC50 Binimetinib (as indicated in the results section) for 33 days. All cells were cultured in RPMI 1640 medium with ultraglutamine (Lonza BioWhittaker, Basel, Switzerland), supplemented with 10% FCS (Fetal Calf Serum, GIBCO ThermoFisher Scientific, Gent, Belgium). In addition, 1% PS (10,000 U/mL Penicillin and 10,000 U/mL Streptomycin, Lonza BioWhittaker, Basel, Switzerland) was added to SKMel30, IPC298, and MelJuso culture media. Cells were maintained at 37°C in a humidified atmosphere containing 5% CO_2 and regularly tested for mycoplasma contamination.

3D melanoma model

Cells were seeded at a density of 0.25 × 10^4 cells/well in RPMI in 96-well Biofloat ULA plates (Facellitate). Drug treatment with respective CDK4/6i (Palbociclib) and MEKi (Binimetinib) amounts and stimulation with 100 μM BzATP (Santa Cruz Biotechnology) started simultaneously 48h post seeding. Drugs and BzATP were replenished every 3–4 days for a total of 14 days. Images were taken before medium change on a Cytation 5 Cell Imaging Multi-Mode Reader (BioTek, Winooski, VT).

At the end of the treatment, cells were lysed and viability was measured with CellTiterGLO 3D Viability assay (Promega) according to the manufacturer's protocol.

METHOD DETAILS

Reagents

MEK inhibitors Binimetinib, Cobimetinib, and Trametinib were purchased from MedKoo Biosciences, MedChemExpress, and Selleck Chemicals (Houston, USA), respectively. CDK4/6 inhibitor Palbociclib was purchased from Selleck Chemicals (Houston, USA) and Ribociclib (LEE011) from Chemietek. P2RX7 antagonists KN-62 and A-740003 were supplied from Selleck Chemicals. Binimetinib, Cobimetinib, Trametinib, Ribociclib, A-740003, and KN-62 were reconstituted with DMSO, and Palbociclib with water according to the manufacturer's instructions. The P2RX7 agonist BzATP triethylammonium salt was purchased from Santa Cruz Biotechnology (Santa Cruz, CA, USA) and reconstituted in water.

Cell viability assays

Dose-response curves and determination of IC50 values

Generation of dose-response curves and determination of half-maximal inhibitor concentration (IC50) values of drugs used in this study were performed in black 96-well μclear plates (Greiner). Briefly, cells were seeded at a density of 0.5×10^4 cells/well in 100 μL of RPMI medium. Drugs were diluted in a 3-fold dilution series, where starting amounts for Palbociclib, Ribociclib, KN-62, and A-740003 were 10 μM, while 1 μM was the initial concentration for Binimetinib, Trametinib, and Cobimetinib. Cell viability was determined with the PrestoBlue Cell Viability Reagent (ThermoFisher Scientific). Upon 3 days of treatment, microplate readers CLARIOstarR (BMG Labtech) and Cytation 5 Cell Imaging Multi-Mode Reader (BioTek, Winooski, VT) were used for measurements of fluorescence intensity. The IC50 experiments were performed in technical and biological triplicates. Dose-response curves and IC50 values were generated with GraphPad Prism 9 and determined with the non-linear log (inhibitor) vs response-variable slope (four parameters) equation. Only results with the R^2 value above 0.92 were considered.

Combination matrix

Both short (3d) and long (30d) treated cells with MEKi plus CDK4/6i therapy were seeded in 96-well black μclear plates at a density of 5,000 cells/well. The concentrations of each inhibitor were pre-defined with respect to each inhibitor's IC50 value. Determined inhibitor amounts were assayed in combined dilution series and at a constant ratio. After 72h of drug exposure, cells were incubated with the PrestoBlue Cell Viability Reagent (ThermoFisher Scientific), microplate readers CLARIOstarR (BMG Labtech) and Cytation 5 Cell Imaging Multi-Mode Reader (BioTek, Winooski, VT) were used for measurements of fluorescence intensity. Percentage of inhibition was calculated using the SynergyFinder software (https://synergyfinder.fimm.fi).[59]

Immunoblotting and antibodies

Cell lysis was performed on ice with cold lysis buffer (30 mM Tris/HCl pH 6.7, 5% glycerol, 2.5% β-mercaptoethanol, and 1% SDS), and protein lysates were further analysed by SDS-PAGE. The detection of enhanced chemiluminescence signals was performed as previously described.[60,61] Primary antibodies used in the study were: anti-phospho-RB (Ser780) (1:1000), anti-RB (1:2000), anti-phospho-ERK1/2 (Tyr202/Tyr204) (1:2000), anti-ERK1/2 (1:1000), anti-phospho-S6 ribosomal protein (pSer235/236) (1:1000), anti-S6 ribosomal protein (1:1000), anti-phospho-MEK (pSER217/221) (1:1000), anti-MEK (1:1000), anti-P2RX7 (E1E8T) (1:1000), and anti-Vinculin (1:1000). All primary and HRP-conjugated secondary antibodies were purchased from Cell Signalling Technology (Boston, MA, USA).

Immunofluorescence staining

Staining with Ki-67 antibody was performed in 8-well μ-slides (Ibidi GmbH). Cells were fixed with 4% PFA. The primary, anti-Ki-67 polyclonal antibody (Abcam, 1:500) was incubated overnight at 4°C. Incubation with secondary Alexa Fluor 647-conjugated donkey anti-rabbit IgG antibody (1:500, Life Technologies) was carried out for 1h at room temperature. DAPI (1:1000, ThermoFisher Scientific, Gent, Belgium) was used for nuclear counterstaining. Olympus IX83 inverted fluorescence microscope was used for detection of Ki-67 immunofluorescence.

Caspase-3 activity assay

To measure caspase-3-mediated apoptosis in untreated and MEKi/CDK4/6i-exposed *NRAS*^{mut} melanoma, cells were seeded in black 96-well μclear plates and treated with single/combined inhibitors for 1 or 4 days. Treatment with staurosporine (10 μM, Cayman chemicals,) for 24h served as positive control. Cells were lysed with a buffer containing 6mM dithiothreitol (6 mM) and 75 mM fluorogenic AC-DEVD-AFC (Santa Cruz Biotechnology, Santa Cruz, CA, USA), for 30 min at RT. Fluorescence intensity of cleaved AFC was measured by the Cytation 5 Cell Imaging Multi-Mode Reader (BioTek, Winooski, VT).

Senescence beta-galactosidase (SA-βgal) activity assay

Senescence was assessed with the β-Galactosidase Staining Kit (Cell Signalling Technology, Boston, MA, USA) following the manufacturer's instructions. Untreated and MEKi and/or CDK4/6i treated cells were seeded onto 24-well plates at 70–80% confluence. Following cell fixation with 1xFixing Solution for 15min, cells were incubated with 1x SA-βgal staining at 37°C overnight. Expression of SA-βGal activity was monitored via color brightfield imaging at 10X magnification on the Cytation 5 Cell Imaging Multi-Mode Reader (BioTek, Winooski, VT).

Real-time proliferation assay

To analyse cell proliferation upon MEKi/CDK4/6i treatment and/or P2RX7 stimulation (100μM BzATP) and/or P2RX7 inhibition (1μM A-740003), 25 × 10^3 MelJuso or SKMel30 cells were seeded in 24- or 12-well plates. Treatments started 24h after seeding and cellular growth was monitored over time by capturing phase contrast images with IncuCyte ZOOM live cell microscope (Essen BioScience).

Single-cell RNA-sequencing

Droplet-based scRNA-Sequencing (Drop-Seq) and droplets generation were performed according to a previously published design of the in-house fabricated microfluidic device.[62,63] All steps of single-cell suspension acquisition and Drop-Seq data pre-processing were performed as previously described.[63]

Single-cell RNA-sequencing data analysis

Drop-Seq data pre-processing

The FASTQ files were assembled from the raw BCL files using the bcl2fastq converter and processed through the FASTQC codes (Babraham bioinformatics) to check for consistency in library qualities. The FASTQ files were then merged and converted into binaries using PICARD's FastqToSam algorithm. The sequencing reads were converted into a digital expression matrix (DGE) using the Drop-Seq bioinformatics pipeline.[64]

Quality filtering of single-cell data

We sequenced a total of 48000 *NRAS*^{mut} melanoma cells (3000 untreated cells and 3000 cells at each time point of treatment (1, 4, and 33 days) for each of the four cell lines). We considered for further analysis the first 1000 cells based on total mRNA to filter out empty beads with damaged cells. We chose this threshold based on visual inspection of the knee plot representing cumulative mRNA count over cell number. The value of 1000 was selected to be after the knee of all time points to assure that we included all high-quality measurements. To test the robustness of this parameter choice we also verified that preliminary results were similar for a value of 800 cells. During quality control, we additionally excluded from further analysis outlier cells that expressed less than 300 and above 8000 genes (Figure S5), this last cut-off to remove measurements that could potentially represent cell doublets. In addition, cells with mitochondrial mRNA content over 15% of the total, or expressing more than 25% of housekeeping genes, or less than 15 housekeeping genes, were considered low-quality and removed for downstream analysis (Figure S5). This finally results in 14883 high-quality cells employed for the study.

Dimensionality reduction and clustering of the scRNA-Seq data

Downstream analysis was performed employing the single-cell analysis tool Seurat v4.0.2. A global-scaling logarithmic normalization method was applied by default Seurat approach.[56] Each normalized matrix was then scaled by a linear transformation to centre the mean gene expression for all cells. The most variable genes were extracted for principal component analysis (PCA). The top PCs were used in further exploration of the data, such as Uniform Manifold Approximation and Projection (UMAP) dimensionality reduction, and clustering. For analysis that included multiple samples, integration through anchoring[56] was applied. A subset of highly variable genes was selected to perform the integration. Differential expression analysis was performed through the FindMarkers function in Seurat, and statistically significant markers were extracted for contrast groups based on an adjusted p-value, with a threshold of 0.05.

Gene set enrichment analysis (GSEA)

Pathway Enrichment Analysis was performed with GSEA 4.0.3 software from the Broad Institute.[57,65] For each analysis, gene set permutations were run 1000 times to obtain a normalized enrichment score (NES). We contemplated results with normalized p-value < 0.05, false discovery rate (FDR) < 0.05, and NES > 1.6. In addition, enrichment analysis was also conducted with fGSEA by using the Hallmark (h.all.v7.5.1.symbols.gmt) and Gene ontology gene sets (c5.all.v7.5.1.symbols.gmt) obtained from the Molecular Signatures Database. Only enriched pathways with adjusted p < 0.05 were considered.

SCENIC

SCENIC analysis was run using the default parameters on (SCENIC v1.2.0).[31] Briefly, we applied GRNboost and RcisTarget packages to identify co-expression between TF binding motifs and target genes. The AUCell package was utilized to calculate regulon enrichment scores. We also checked the regulon specificity score (RSS)[66] by SCENIC calsRSS function.

Pseudotime inference

Slingshot pseudotime[21] and Monocle2 pseudotime[24] were applied to assess cell lineage and pseudotemporal cell ordering.

RNA extraction and quantitative PCR

Total RNA was isolated from three biological replicates each consisting of technical triplicates using the Quick-RNA™ Mini-Prep Kit (ZYMO Research, Irvine, CA, USA), according to the manufacturer's instructions. RNA was quantified with NanoDrop2000 Spectrophotometer (Isogen Life Science, Utrecht, The Netherlands). The iScriptTM cDNA Synthesis kit (Bio-Rad, Hercules, CA, USA) was utilized for cDNAs synthesis. Quantitative real-time PCR (qPCR) and analysis was carried out as previously described.[67] The sequences of primers (5′→3′) used in this study were P2RX7 (F: CGGAAAGAGCCTGTCATCA; R: TGTAGTCTGCGGTGTCAAAGA), HPRT (F: TGGACAGGACTGAACGTCTT; R: GAGCACACAGAGGGCTACAA), TBP (F: TGATCTTTGCAGTGACCCAG; R: CGCTGGAA CTCGTCTCACTA), PPIA (F: CAGACAAGGTCCCAAAGACA; R: CCATTATGGCGTGTGAAGTC).

Small interfering RNAs and transfection

P2RX7 siRNA was obtained from Horizon Discovery. siRNA transfections were performed using Lipofectamine RNAiMAX (Invitrogen, Thermo Fisher Scientific, Gent, Belgium) according to the manufacturer's instructions. Cells were transfected 24h after MEKi/CDK4/6i-treatment initiation with 20 nM siRNA or Negative Control (NC) for a total of 72h.

Flow cytometry and ROS activity

The generation of reactive oxygen species (ROS) was quantified with the fluorogenic probe 5-(and 6)-chloromethyl-2′,7′-dichlorodihydrofluorescein diacetate (CM-H2DCFDA) (Thermo Fisher Scientific, Gent, Belgium), used at a concentration of 5 μ M. 400 μ M hydrogen peroxide (Carl ROTH, Karlsruhe, Germany) served as positive control. Dead cell populations were excluded by staining with Live/Dead Fixable Near-IR Dead Cell stain (Thermo Fisher Scientific, Gent, Belgium). CM-H2DCFDA fluorescence was measured by Flow Cytometry and analysed by FlowJo v10.8.1 software.

Seahorse and real-time ATP rate assay

Seahorse XFe96 analyser (Agilent Technologies) was used to measure Oxygen Consumption Rate (OCR) and Extracellular Acidification Rate (ECAR). Obtained values were used to calculate ATP production rate from glycolysis and mitochondria. Briefly, cells were seeded in a poly-D-lysine coated Seahorse 96-well plate in RPMI. On the day of the assay, cells were washed with Seahorse XF RPMI (pH 7.4) supplemented with 10 mM glucose, 2 mM glutamine, and 1 mM pyruvate, and incubated in a non-CO2 incubator at 37°C for 1h. Sequential injections of 1.5 μM Oligomycin and 0.5 μM Rotenone/AntimycinA allowed calculation of glycolytic and mitochondrial ATP production rates according to manufacturer's instructions. For measurements with BzATP, 100 μM final concentration was injected preceding Oligomycin and Rotenone/AntimycinA.

ATP consumption and production assay

To measure the ATP production and consumption rates, we utilized the ATP Determination Kit (ThermoFisher Scientific). To determine ATP consumption rates, we stimulated untreated and 1d/4d-treated cells with 2 μM ATP in HBSS with Calcium and Magnesium (+/+) (Gibco, ThermoFisher Scientific) and followed the manufacturer's protocol to determine consumed ATP amounts corresponding to ATP leftovers in the supernatants. Upon 1h of ATP addition, 10 μL of supernatant was transferred to a white 96-Lumitrac plate (Greiner) to proceed with luciferase measurements. ATP production rates were estimated directly from 10 μL of HBSS +/+ supernatant from untreated, 1d- and 4d-treated cells, without additional ATP stimulation. Simultaneously with luciferase measurements, we performed nuclei staining with Hoechst 33342 (ThermoFisher Scientific) on the attached cells for normalisation purpose. Luciferase measurements and fluorescent reading were done on the Cytation 5 Cell Imaging Multi-Mode Reader (BioTek, Winooski, VT).

Survival analysis

We utilized the cBioPortal database (http://www.cbioportal.org) to obtain skin cutaneous melanoma data from the Cancer Genome Atlas (TCGA, PanCancer data) and assess the effect of P2RX7 mRNA expression on the overall and progression-free survival of *NRAS*^{mut} and *BRAF*^{mut} melanoma patients. Upon patient stratification based on P2RX7 median expression, corresponding Kaplan-Meier survival curves were plotted in cBioPortal.

Human melanoma samples and P2RX7 immunohistochemistry

Anonymized formalin-fixed and paraffin-embedded (FFPE) tissue samples from routine diagnostics were subjected to P2RX7 immunohistochemistry. The use of fully anonymized human material was approved by the ethics committee (CNER (Comité national d'éthique de recherche), reference Nr. 1121-278). Minimal clinical data such as age, sex and final pathological diagnoses were included (see Table S6). In brief, immunohistochemistry was performed on 2–3 μm thick slices of 14 melanoma patients (*NRAS*^{mut}: n=5; *BRAF*^{mut}: n=5; wild-type: n=4) on the automated IHC staining system Dako Omnis (Agilent, Santa Clara, California, USA) using rabbit-anti-human-P2RX7 antibody HPA034968 (MERCK Life Science BV; 1:500). The staining procedure included heat and chemical treatment of the slides with EnVision FLEX TRS at low pH at 97°C (30 min), incubation with primary rabbit-anti-P2RX7 antibody (20 min) and 3 min endogenous enzyme block with EnV FLEX Peroxidase-Blocking solution. Signal enhancement was achieved by incubating slides with EnV Flex + Rabbit LINKER (10 min). EnV FLEX/HRP labeled polymer (20 min) was used as secondary antibody, followed by incubation with the EnVision FLEX HRP Magenta Substrate Chromogen for 5 min. Slides were counterstained with hematoxylin and mounted with coverslipping film Tissue-Tek (Sakura, Staufen, Germany). Slides were then scanned in the Philips IntelliSite Pathology Solution Ultrafast Scanner 1.6, digitized, and transferred to a computer screen. Brightness, gain, and contrast were all kept constant during image acquisition. Melanoma tissue and normal skin adjacent to the tumour tissue were then assessed for immunoreactivity (negative, weak, moderate, or strong) to P2RX7 (see also Figure S14).

QUANTIFICATION AND STATISTICAL ANALYSIS

One-way ANOVA followed by multiple comparison tests was employed to conduct statistical analyses. P-values equal to or less than 0.05 were considered significant. The figure legends contain the information regarding the number of biological replicates and the statistical details for each analysis. All the methods for scRNA-seq data analysis are described in section: single-cell RNA-sequencing data analysis.